EXPERIMENTAL ANALYSIS OF WELD BEAD GEOMETRY IN SYNERGIC MIG WELDING OF 304L STAINLESS STEEL

Submitted
by

RAVI BUTOLA
(Roll No. : **2K11/PIE/16**)
Mechanical Engineering Department

In partial fulfillment of the requirement of the degree of
MASTERS OF TECHNOLOGY

In

Production Engineering

Under the guidance of:

Mr. M.S. NIRANJAN

Assistant Professor

Department of Mechanical Engineering

Department of Mechanical Engineering

DELHI TECHNOLOGICAL UNIVERSITY

(Formerly Delhi College of Engineering)

Bawana Road, New Delhi

CERTIFICATE

Date:-_____

This is to certify that report entitled "Experimental analysis of Weld Bead Geometry in synergic MIG welding of 304L stainless steel" by Mr. Ravi Butola is the requirement of the partial fulfillment for the award of Degree of Master of Technology (M. Tech.) in Production Engineering at Delhi Technological University. This work was completed under my supervision and guidance. He has completed his work with utmost sincerity and diligence. The work embodied in this project has not been submitted for the award of any other degree to the best of my knowledge.

Guide

Mr. M.S NIRANJAN

Assistant Professor

Department of Mechanical Engg

DTU, Delhi

Co-Guide

Dr. KASIM MURTAZA

Associate Professor

Department Mechanical Engg

DTU, Delhi

ACKNOWLDGEMENT

To achieve success in any work, guidance plays an important role. It makes us put right amount of energy in the right direction and at right time to obtain the desired result. I express my sincere gratitude to my guides, **Mr. M.S. NIRANJAN,** Assistant Professor, Mechanical Engineering Department for giving valuable guidance during the course of this work, for their ever encouraging and timely moral support. Their enormous knowledge always helped me unconditionally to solve various problems.

I am greatly thankful to **Dr. Naveen kumar**, Professor and Head, Mechanical Engineering Department, Delhi Technological University, for his encouragement and inspiration for execution of the this work. I express my feelings of thanks to the entire faculty and staff, Department of Mechanical Engineering, Delhi Technological University, Delhi for their help, inspiration and moral support, which went a long way in the successful completion of my report work.

RAVI BUTOLA

(Roll No. 2K11/PIE/16)

ABSTRACT

The experimental study is carried out for the analysis of weld bead geometry such as bead reinforcement height, bead width and bead penetration of synergic MIG welding of 304L stainless steel. The mechanical strength has been tested on UTM and found that the strength of welds is influenced by the composition of metal, weld bead geometry and shape relationship. It was observed that the yield strength and ultimate tensile strength of the weld metal is less than the base metal. It was also observed that the percentage elongation of welded specimen is 89.126% where as the base specimen is 76.3%. Therefore, the ductility of welded specimen is higher than the base metal.

Metallurgical investigations determine the variation of micro hardness across the weld metal zone, heat affected zone and the base metal. Vickers micro hardness is carried out to determine the hardness values at various zones. It was observed that the hardness value is maximum for base metal and minimum in the HAZ region it is also observed that the hardness values tested at different points in fusion zone and found more than hardness value in HAZ region.

Microstructures of different zones of interest like weld metal, HAZ and fusion boundary under different welding parameters were viewed and captured with an optical microscope coupled with an image analyzing software. Fractured ends of the weld bead specimens were analyzed using Scanning electron microscopy (SEM) to the nature of the fracture mode. The results of EDS analysis shows that the inclusion particle mainly composed of Fe, Cr, Mn, Si, C elements.X ray diffraction (XRD) study has been done and result shows that phases like Fe, Ni-Cr-Fe, and Fe-Cr-Co-Ni are determined.

Keywords: weld bead, mechanical properties, metallurgical investigation, micro hardness, SEM, XRD.

CONTENTS

LIST OF FIGURES

LIST OF TABLES

CHAPTER 1

INTRODUCTION

1.1 Introduction

Gas Metal Arc Welding is a process in which the source of heat is an arc format between consumable metal electrode and the work piece, and the arc and the molten puddle are protected from contamination by the atmosphere (i.e. oxygen and nitrogen) with an externally supplied gaseous shield of gas either inert such as argon, helium or an argon-helium mixture or active such as carbon dioxide, argon-carbon dioxide mixture, which is chemically active or not inert [1]. Initially GMAW was called as MIG Welding because only inert gasses were used to protect the molten puddle. The application of this process was restricted to aluminum, deoxidized copper and silicon bronze. Later it was used to weld ferrite and austenitic steels, and mild steel successfully by using active gasses in place of inert gasses and hence was term MAG (Metal Active Gas) welding [2]. All the major commercial metals can be welded by GMAW (MIG/CO_2) process, including carbon steels, low alloy and high alloy steels, stainless, aluminum, and copper titanium, zirconium and nickel alloys. [3]. GMAW welding process overcome the restriction of using small lengths of electrodes and overcome the inability of the submerged-arc process to weld in various positions. By suitable adjusting the process parameters, it is possible to weld joints in the thickness range of 1-13 mm in all welding position.

Influence of heat input on microstructure and mechanical properties of GMAW welding of 304L stainless steel bead geometry was studied. Three heat input combination designated as low heat, medium heat and high heat were selected from the window of GMAW welding process and weld joint made using these combinations were subjected to microstructure, tensile testing ,scanning electron microscope and x-ray diffraction so as to analyze of the weld bead.

Several researchers have attempted to investigate the effects of various process variables on the weld bead geometry and metal transfer. The quality of any

weld process is characterized by the weld distortion, mechanical properties and weld bead geometry. Out of these factors, the weld bead geometry is the easiest to measure and control. Thus by controlling the weld bead geometry we can successfully control the weld quality. But the relationship between the process variables and the weld bead geometry is very complex and necessitates a robust mathematical approach to quantify the relationship between them.

Synergic MIG is an advanced welding system which incorporates both spray and pulse transfer. It is a complete range of high technology digital microprocessor controlled equipment. Optimum conditions can be established for a range of applications which are readily reproduced by the welder. Synergic means "to work together" and in connection with the welding process it indicates that the welding machine is capable of choosing the current curve when the welder has set the wire speed, the metal alloy, the wire diameter and the shielding gas. That is the welding equipment controls the base current, the form and number of the current pulsations. The synergic

capability enabled all of the welding parameters to be controlled from a signal dial control which optimized the current peak pulse and background Values, the voltage, wire feed speed. It has also become possible to reprogram the power source instantly when wire size, shield gas, filler metal composition, etc.

Bead geometry (bead height and width) and penetration (depth and area) are important physical characteristics of a weldment. Several welding parameters seem to affect the bead geometry and penetration. It was observed that high arc-travel rate or low arc-power normally produced poor fusion. Higher electrode feed rate produced higher bead width making the bead flatter.

Apart from influencing the bead geometry, the input process variables also affect the metallurgical aspects of the metal being joined. The micro hardness, the different phases constituting the micro structure, the percentage of different phases, grain size etc. are largely influenced by the input process variables and ultimately they affect the performance of the welded metal in different applications.

The micro hardness (VHN) test was performed on the etched traverse cross-section of the Synergic MIG weld zone using a load of 100 gm, which was applied for

duration of 10 sec. seven measurement in each sample of weld zone including base material, weld bead and heat affected zone (HAZ) were taken at regular intervals.

The main aim of the tensile test is to evaluate the strength and plasticity of welding joints and examine the influence of welding defects on the joint performance. The test is done on computer interface electronic universal testing machine. The transverse tensile strength, yield strength and percentage of elongation of all joints have been evaluated.

The properties of metals highly depend on their structures. The internal structures determine how materials perform under a given application. The effects of most industrial processes applied to metals to control their properties can be explained by studying their microstructures.

The most common method used to examine the structures of materials is optical technique. A specimen about 20mm on an edge is cut from the metal to be examined. A mirror polish is produced on one face of the specimen by grinding on successively fine emery (sand) papers and polishing on revolving cloth wheels with fine abrasives such as alumina powder. To reveal the structural details such as grain boundaries, phases and inclusions this polished surface is etched with chemical solutions. The etchant attacks various parts of the specimen at different rates and reveals the structure. A metallographic microscope is used to examine the microstructure.

In scanning electron microscopy (SEM), the second category, the surface of the specimen is bombarded with a beam of electrons to provide information for producing an image. SEM is used to characterize structure by revealing grain boundaries, phase boundaries, inclusion distribution, and evidence of mechanical deformation. Scanning electron microscopy is also used to characterize fracture surfaces, corrosion products, and other rough surfaces, especially when elemental microanalysis of small features is desired.

Energy Dispersive X-ray analysis (EDX) referred to as EDS or EDAX, is an x-ray technique used to identify the elemental composition of materials.EDX systems are attachment to SEM and TEM instruments where the imaging capability of the microscope identifies the specimen of interest .The data generated by EDX analysis consist of spectra showing peaks Corresponding to the elements making up the true

composition of the sample being analysed. This technique is used in conjunction with SEM and is not a surface science technique. An electron beam strikes the surface of a conducting sample. The energy of the beam is typically in the range 10-20keV. This causes X-rays to be emitted from the point the material. The energy of the X-rays emitted depends on the material under examination. The X-rays are generated in a region about 2 microns in depth, and thus EDX is not a surface science technique. By moving the electron beam across the material an image of each element in the sample can be acquired in a manner similar to SEM.

X-ray diffraction (XRD) uses x-rays to investigate and quantify the crystalline nature of materials by measuring the diffraction of x-rays from the planes of atoms within the material. It is sensitive to both the type of and relative position of atoms in the material as well as the length scale over which the crystalline order persists. It can, therefore, be used to measure the crystalline content of materials; identify the crystalline phases present (including the quantification of mixtures in favourable cases); determine the spacing between lattice planes and the length scales over which they persist; and to study preferential ordering and epitaxial growth of crystallites.

1.2 Motivation and objective

The motivation of this project was provided by desire to explore the frontiers of welding technology, which form the backbone of manufacturing industries. To be able to successfully use a process in industry it is imperative that we have a robust way of controlling the outputs as per our needs.

The main objective of this project was to understand the influence of Metallurgical investigations determine the variation of micro hardness across the weld metal zone, heat affected zone and the base metal. Vickers micro hardness is carried out to determine the hardness values of the metal at various zones. Also the microstructure of the resultant welded metal was co-related with the process variables.

A scanning electron microscope (SEM) is a type of electron microscope that produces images of a sample by scanning it with a focused beam of electrons. The electro interact with electrons in the sample, producing various signals that can be detected

and that contain information about the sample's surface topography and composition.

Energy Dispersive X-ray analysis (EDX) referred to as EDS or EDAX, is an x-ray technique used to identify the elemental composition of materials. The data generated by EDX analysis consist of spectra showing peaks corresponding to the elements making up the true composition of the sample being analysed.

Tensile test is to evaluate the strength and plasticity of welding joints and examine the influence of welding defects on the joint performance.

1.3 Statement of the Problem

"Experimental analysis of Weld Bead Geometry in synergic MIG welding of 304L stainless steel"

The research work describes the experimental observations made on 304L stainless steel welded plate through bead-on-plate and the metallurgical aspects in the weld bead geometry, the input process variables also affect the metallurgical aspects of the metal being joined. The micro hardness, the different phases constituting the micro structure, fracture surfaces, elemental composition of materials, the percentage of different phases, grain size etc. are largely influenced by the input process variables and ultimately they affect the performance of the welded metal in different applications.

1.4 Plan of Investigation

The research work was planned to be carried out in following steps:

1. Identification of important process control variable.

2. Deciding the working range of process control variable, viz. welding current (A), plate thickness(T), gas flow rate(G), and Travel speed(S)

3. Recording the responses of optimum parameter of viz. bead height(H), bead width(W),bead penetration (P)

4. Prepare Bakelite sample using Simplimet 100 Automatic Mounting Press.

5. Finding micro structure and micro hardness.

6. Tensile test of welded specimen

7. Test on scanning electron microscope(SEM) and EDS

8. X- ray diffraction(XRD) test

CHAPTER 2
LITERATURE REVIEW

2.1 Introduction

Welding is a fabrication process that joins two metals or non-metals by producing coalescence between them. This is generally achieved by heating the specimen up to their melting temperature with or without the addition of filler materials, to form a pool of molten metal that cool and solidifies to become a strong joint. While often an industrial process, welding can be done in many different environments, including open air, under water and in outer space. The studies of the effects of various welding process parameters on the formation of bead and bead geometry have attracted the attention of many researchers to carry out further investigations.

Many researchers and academicians of international repute have probed into the topic of study of weld geometry and the mechanical performance and application of any welded joint is affected by the metallurgical properties of the welded joints. The present literature review has been carried out in the areas concerning the influence of input process variables in the bead geometry.

Significant grain coarsening was observed in the heat affected zone (HAZ) of all the joint and it was found that the extent of grain coarsening in the heat affected zone increased with increase in the heat input. For the joint investigation in this study it was also found that average dendrite length and inter-dendrite spacing in the weld zone increase with increase in the heat input which is the main reason for the observable changes in the tensile properties of the weld joint.

Austenitic stainless steels have been used widely by the fabrication industry owing to their excellent high temperature and corrosion resistance properties. Some of the typical applications of these steel include their use as nuclear structural material for reactor coolant piping, valve bodies, vessel internals, chemical and process industries, dairy industries, petrochemical industries etc. Out of 300 series grade of these steels type 304 SS is extensively used in industries due to its superior low temperature

toughness and corrosion resistance. One of the typical applications of type 304 SS include storing and transportation of liquefied natural gas (LNG), whose boiling point is −162 °C under 1 atmosphere.

A study on fatigue crack growth rate for type 304 SS over a temperature range from room to −162 °C has shown that base metal possesses superior resistance to crack growth relative to weld metals over the entire temperature range. Another typical application of this material includes its use as bellows used as conduit for liquid fuel and oxidizer in propellant tank of satellite launch vehicle.

Other studies which show that 304 SS and 304L SS grade has been the topic of research of many researchers include various studies like experimental determination of grain boundary composition of 304 SS in low temperature sensitization condition using a scanning Auger microprobe, measuring chromium depletion after various thermal heat treatments, modeling of low temperature sensitization of austenitic stainless steel, studying sensitization behavior of grain boundary engineered austenitic stainless steel, arresting weld decay in 304 SS by twin-induced grain boundary engineering.

Influence of heat input on microstructure and mechanical properties of GMAW welding of 304L stainless steel bead geometry was studied. Three heat input combination designated as low heat, medium heat and high heat were selected from the window of GMAW welding process and weld joint made using these combinations were subjected to microstructure, micro hardness, tensile testing ,scanning electron microscope and x-ray diffraction so as to analyze of the weld bead.

Micro structure of different zones of interest weld metal, HAZ and fusion boundary under different heat input combinations were viewed and capture with an optical microscope coupled with image an image analyzing software. Micro hardness of different zones of weldment was measured using vicker's micro hardness testing machine with a lode of 100 gm. Fracture end of the specimens were analyzed using scanning electron microscope (SEM) to assess the nature of fracture mode.

From the literature reviewed on the material processing of 304 SS it is observed that no systematic work on the effect of heat input on microstructure and tensile properties

of gas tungsten arc (GTA) welded has been reported. In view of the fact that arc welding processes like GTAW offer a wide spectrum of thermal energy for joining different thicknesses of steels it was considered important that undertaking the present study would be beneficial in gaining an understanding about the metallurgical aspects that affect the service performance of these welded joints made using different heat input combination.

Chen et al. [4] **:** found that when Cu–Si enriched type 304 SS (containing2–2.5 wt. % copper and 1–1.5 wt.% silicon) and a conventional type 304 SS was Welded using gas metal arc welding (GMAW), process ductility decreased and   Ferrite levels increased in both weldments, as the heat input was increased.

Yan et al. [5] **:** on the microstructure and mechanical properties of 304 SS   joints by tungsten inert gas (TIG) welding, laser welding and laser- TIG hybrid welding showed that laser welding could give highest tensile strength and smallest dendrite size in all joints whereas TIG welding gave lowest tensile strength and biggest dendrite size

Muthupandi et al. [6]**:**   on the effect of weld chemistry and heat input on the structure and properties of duplex stainless steel welds using Autogenous-TIG and electron beam welding process shows that chemical composition exerts a greater influence on the ferrite–austenite ratio than the   cooling rate.

Jana [7] **:** has reported the effect of varying heat inputs on the properties of the HAZ of Two different duplex steels and found that as arc energy increased hardness of both weld metal and the HAZ decreased, whereas width of the HAZ   increased with increased arc energies

Kim I.S., Basu A and siores E.[8] studied the effect of welding process parameters on weld bead penetration Gas Metal Arc Welding (GMAW) process. Welding process parameters included wire diameter, gas flow rate, welding speed, arc current and arc voltage. The experiment results revealed that weld bead penetration increased as wire diameter, arc current and voltage increased

D.S. Nagesh, G.L. Datta [9]   Both the bead height and width decrease with the increase in arc-travel rate but   the decrease in height is comparatively more to make

a flatter bead with a higher arc-travel rate. An increase in   arc-length keeping electrode feed   rate constant results in an increase in bead width and decrease in bead height. The penetration and HAZ increase with the increase in electrode feed rate keeping arc-length constant.

Kim I.S, Son K.J., Yang and Yaragada [10] developed a mathematical model for selection of process parameters and prediction of bead geometry in robotic GMAW. They used factorial design as a guide for optimization of process parameters. Three factors were incorporated into the model: arc current welding voltage and welding speed. The study revealed that a change of process parameters effects the bead width and height more strongly than penetration relatively.

Reeta Wattal and S. Pandey [11] concluded that the mode of metal transfer is mainly by type of arc, welding current, electrode polarity, arc voltage, NTP, gas compositions, gas flow rate.

Zumelzu et al, [12] studied the mechanical behavior of AISI 316L welded joints using shielded metal arc welding (SMAW) and (GMAW) process with different electrodes types. Their work concludes that a direct correction exists between the thermal contribution and tensile strength for the materials studied. The effect of minor element and shielding gas on the penetration of TIG welding in type 304 ss have been studied using bead on plate experimentation technique and it is conclude that minor element such as oxygen, aluminum and sulfur have a significant effect on the weld depth to width ratio.

Yan et al [13] analyzed the study on microstructure and mechanical properties of 304 stainless steel joints by TIG, laser and laser-TIG hybrid welding and reported that the join by laser welding had highest tensile strength and smallest dendrite size in all joints, while the joint by TIG welding had lowest tensile strength, biggest dendrite size. The laser welding and hybrid welding are suitable for welding 304 stainless steels owing to their high welding speed and excellent mechanical properties.

El Batahgy [14] investigated the effects of austenitic stainless steels on surface of hardness and fusion zone of laser welding parameters and indicated that penetration

increased depending on the increased welding power and welding speed, a significant difference between helium and argon shielding gases was not observed, and mechanical properties (tension, hardness, bending) and fusion zone were not affected by heat input at room temperature.

Ventrella et al [15] analyzed the pulsed laser seam welding of AISI 316L stainless steel thin foils and reported that pulse energy control is of considerable importance to thin foil weld quality because it can generate good mechanical properties and reduce discontinuities in weld joints. The ultimate tensile strength of the welded joints increased at first and then decreased as the pulse energy increased. The process appeared to be very sensitive to the gap between couples.

Zambon et al. [16] made analyses related the microstructure and tensile stages of AISI 904L super austenitic stainless steel on CO_2 laser welding and demonstrated that in flow resistance and detach tensile a decrease was observed and depending on this decrease, there was also an increase in hardness value because of rapid cooling of the fusion zone during welding.

Ames et al. [17] compared the austenitic (316L), super austenitic (254SMO) and super duplex (SAF 2507) weld properties produced using GTAW flux. The microstructure, mechanical properties and corrosion resistance of such welds were compared also to autogenous welds produced using the current industry standard gas (argon). In all cases, the welds produced with GTAW flux exhibited equivalent or improved microstructure and properties when compared to the autogenous non-flux welds. Depending on the amount of cold work present, the strength and hardness in the HAZ and FZ softened due to the weld thermal cycle. Micro hardness traverses across welds examined in [17] showed this softening effect.

Lee et al. [18] have reported in their studies on effects of strain rate and failure behaviour of 304L SS SMAW weldments and find that as the strain rate increases, the flow stress increases and the fracture strain decreases.

Milad et al. [19] found that yield and tensile strengths of 304 SS increased gradually at the same rate with increasing degree of cold work.

Shyu et al. [20] have investigated the effect of oxide fluxes on weld morphology, arc voltage, mechanical properties, angular distortion and hot cracking susceptibility of autogenous TIG bead on plate welds. Their results indicate that penetration is significantly increased which in turn increases depth to bead-width ratio and tends to reduce angular distortion.

Ghani et al [21] analyzed the micro structural characteristics of low carbon steels on Nd: YAG laser welding and reported that depending on the increased energy input and process speed, the hardness value of the material at welding zone also increased.

Venugopal et al. [22] and **Sundaraman et al**. [23] discussed the workability and microstructure of 304L stainless steel at low strain rates. However, as strain rate increases up into the dynamic range, the plastic deformation of 304L stainless steel and corresponding microstructures evolution is obviously different from static or quasi-static loading conditions.

Hecker et al. [24] and **Murr et al**. [25] concluded that the volume fraction of martensite under high strain rates is greater than that under low strain rates at specific low strain conditions. However, with increasing strain, heat effects induced by large deformation under high strain rate restrict the transformation of martensite. Effects of dislocation and transformed martensite likewise influence the mechanical behaviour of 304L stainless steel under high strain rate loading. Thus, this paper aims to characterize 304L stainless steel plastic deformation under high strain rates at room temperature, and to propose a constitutive model to describe the experimental strain–stress curve. The relationship between dislocation density, cell size, magnitude of transformed martensite, flow stress and strain rate will be determined and discussed in terms of observed microstructure.

Di Caprio *et al*. [26] 1997, Super austenitic stainless steel (AISI 904 L) is a highly alloyed austenitic low carbon stainless steel having good weldability. Due to its high molybdenum content and specially designed welding consumables with low impurity level, hot crack formation during welding can be avoided despite the fully austenitic

filler metal. Super austenitic stainless steel (AISI 904 L) is primarily characterized by its excellent ductility, even at low temperatures. Ferrite free, fully austenitic stainless steel with high nitrogen content has very good impact strength and is therefore very suitable for cryogenic applications. Especially for nitrogen alloyed steel, yield and tensile strengths are generally high.

M. Eroglu et al [27] carried out investigations to study the effect of coarse initial grain size on microstructure and mechanical properties of weld metal and HAZ of low carbon steel. In this study, the effects of coarse initial grain size with varying heat inputs on microstructure and mechanical properties of weld metal and heat- affected zone (HAZ) were investigated. Microstructure, hardness and toughness of weld metals and HAZs were investigated. From the results, they tried to establish a relationship between initial grain size, microstructure, hardness and toughness of weld metals and HAZs. Considering the heat input, it was observed that the coarse initial grain size had a great influence on the microstructure, hardness and toughness of HAZ of low carbon steel. Thus, taking into consideration the plate thickness, a higher heat input should be used with respect to the maximum toughness of the HAZ in the welding of grain-coarsened low carbon steels.

Ludwik [28] proposed a simple model that considered only the effect of work hardening on the stress–strain curve. Ludwik's early attempt was soon found an insufficient description. Other workers soon included the effects of strain rate and temperature on a material's plastic deformation.

The present research works have done on experimental analysis of weld bead geometry in synergic MIG welding of 304L stainless steel. On the basis of literature review it is observed that independent work has been done in experiment of Synergic MIG welding process, their analysis and metallurgical studies have been carried out independently. But an integrated approach of studying the effects of various welding process variables on bead geometry of welding plates, use of micro structure, micro hardness, Tensile test, SEM, EDX and XRD of the weld bead geometry and studying the influence of process parameters on the metallurgy of the welded specimen in MIG welding of plates is hardly found in any literature.

CHAPTER 3

EXPERIMENTATION

3.1 MIG Welding

3.1.1 Introduction

Gas Metal Arc Welding is a process in which the source of heat is an arc format between consumable metal electrode and the work piece, and the arc and the molten puddle are protected from contamination by the atmosphere. The American Welding Society refers to the process Gas Metal Arc Welding process to cover inert as well as active shield gasses. GMAW is basically a semi-automatic process, in which the arc lengths of electrode and the feeding of the wire are automatically controlled.
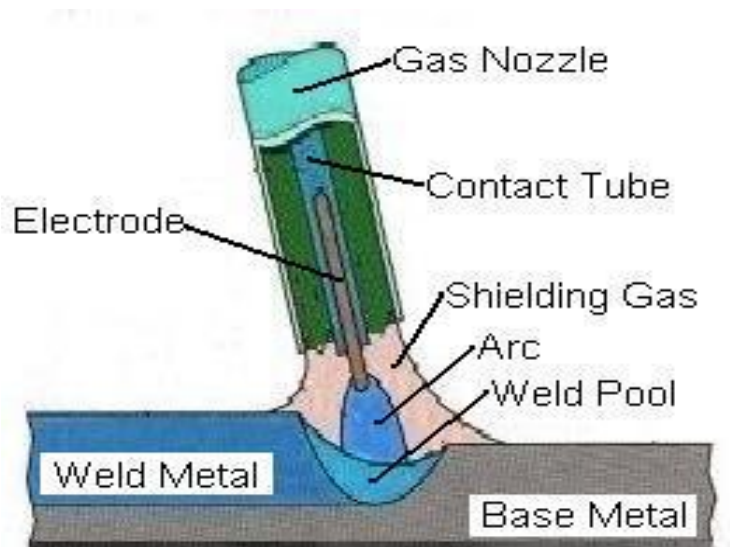

Figure: 3.1 Fundamental features of the MIG process.

The welding operator's job is reduced to positioning the gun at a correct angle and moving it along the seam at a controlled travel speed. Hence less operator skill is required with this process as compare to TIG and manual metal arc process. Yet basic training is required in the setting up of the equipment and manipulation of the gun must be provided to the operator to ensure quality GMAW welding [12, 13]. GMAW welding process overcome the restriction of using small lengths of and overcome the inability of the submerged-arc process to weld in various positions electrode.

By suitable adjusting the process parameters, it is possible to weld joints in the thickness range of 1-13 mm in all welding position [14]. All the major commercial metals can be welded by GMAW (MIG/CO2) process, including carbon steels, low alloy and high alloy steels, stainless, aluminum, and copper titanium, zirconium and nickel alloys.

Figure: 3.2 General arrangement of the power source, wire feeder gas cylinder and work area

The MIG welding process, illustrated in figs.3.1 and fig.3.2. As a rule uses direct current with the electrode connected to the positive pole of the power source, DC positive, or reverse polarity in the USA. Recent power source developments have been successful in enabling the MIG process to be also used with AC. Most of the heat developed in the arc is generated at the positive pole, in the case of MIG welding the electrode, resulting in high wire burn-off rates and an efficient transfer of this heat into the weld pool by means of the filler wire.

3.1.2 SYNERGIC MIG WELDING

Synergic MIG/MAG is an advanced welding system which incorporates both spray and pulse transfer. Optimum conditions can be established for a range of applications which are readily reproduced by the welder. Synergic means "to work together" and in

connection with the welding process it indicates that the welding machine is capable of choosing the with current curve when the welder has set the wire speed, the metal alloy, the wire diameter and the shielding gas. That is the welding equipment controls the base current, the form and number of the current pulsations.

The synergic capability enabled all of the welding parameters to be controlled from a signal dial control which optimized the current peak pulse and background values, the voltage, wire feed speed. It has also became possible to reprogramme the power source instantly when wire size, shield gas, filler metal composition, etc. are changed, simply by dialing in a programme number .These programmes have been established by the equipment manufacturer with the optimum parameters for the application. Initially these units were expensive but the price has been steadily reduced such that they are now only marginally more costly than a conventional power source, leading to a far wider usage.

3.1.3 MECHANISM OF METAL TRANSFER

The **short-circuiting** or **dip transfer** mode, in which the metal melts to form large droplets whose diameter is often greater than that of the electrode wire. As the droplet forms at the end of the electrode, it makes contact with the weld pool and creates a short circuit, with a sudden increase in current. The surface tension causes a pinching effect which separates the droplet from the electrode. The frequency of this phenomenon is of the order of 20 to100 Hz, corresponding to cycle times between 0.01 and 0.05 seconds.
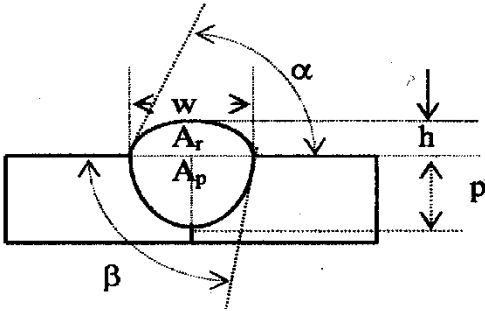
The **globular transfer** or **gravity transfer** mode, as in the previous case, melting occurs in the form of large droplets, which break away when their mass is sufficient to overcome surface tension forces and due to the greater arc length, fall freely before coming into contact with the weld pool.

The **spray transfer** mode involves current densities above a certain transition level, of the order of 200 A /mm^2. The electrode melts to give a stream of fine droplets. As the current density increases further, the electrode tip becomes conical and the stream of even finer droplets is released axially.

3.1.4 WELD BEAD GEOMETRY

The mechanical properties of the welded joints greatly depend on weld bead geometry which in turn, is influenced by welding parameters like arc current, arc voltage, and arc travel speed. The bead geometry is specified by weld bead width, reinforcement height, reinforcement area, penetration height, penetration area and the contact angle of weld bead etc.

Table no: 3.1 Bead geometry

	Ap	Area of penetration
$$\%D = \frac{A_p}{A_t}100 = \% \text{ dilution}$$	Ar	Area of reinforcement
	α	Angle of convexity
	β	Angle of entry
	A_t	$A_p + A_r$ Total weld bead area

The Weld Bead Width is the maximum width of the weld metal deposited. It increases with arc current, arc voltage; electrode weaving and decreases as arc travel speed increases. Penetration Height or simply penetration is the distance from base plate top surface to the maximum extent of the weld nugget. Penetration determines the load carrying capacity of a welded structure. Penetration Area is that covered by the fusion line below the base metal level. Penetration area affects the weld strength. Reinforcement Height is the maximum distance between the base metal level and the top point of the deposited metal. Reinforcement Area is one included between the

contour line of the deposited metal above the base metal level.

3.1.5 TYPES OF STAINLESS STEELS

There are three basic types of stainless steels:

• Austenitic (200 and 300 Series)

• Ferritic (some of the 400 Series)

• Martensitic (balance of the 400 Series)

Austenitic stainless steels are iron-chromium-nickel alloys which are hardenable only by cold working. Nickel is the main element varied within the alloys of this class while carbon is kept to low levels. The nickel content may be varied from about 4% to 22% - higher values of nickel are added to increase to ductility of the metal. When chromium is increased to raise the corrosion resistance of the metal, nickel must also be increased to maintain the austenitic structure.

The ferritic stainless steels are ferromagnetic and have better resistance to stress-corrosion cracking, pitting, and crevice corrosion than the austenitics. The martensitics contain higher levels of carbon, which gives them very high strength. The duplex stainless steels contain two metallurgical phases at room temperature (austenite and ferrite), and thus they have some of the best properties of each.

Table no: 3.2 Typical Analysis in Percent: [15]

Type	UNS	C	Cr	Ni	Mn	Si	S	P	Mo
302	S30200	.15	17-19	8-10	2.0	1.0	.03	.04	
304	S30400	.08	18-20	8-12	2.0	1.0	.03	.04	
304L	S30403	.03	18-20	8-12	2.0	1.0	.03	.04	
316	S31600	.08	16-18	10-14	2.0	1.0	.03	.04	2.0-3.0
316L	S31603	.03	16-18	10-14	2.0	1.0	.03	.04	2.0-3.0
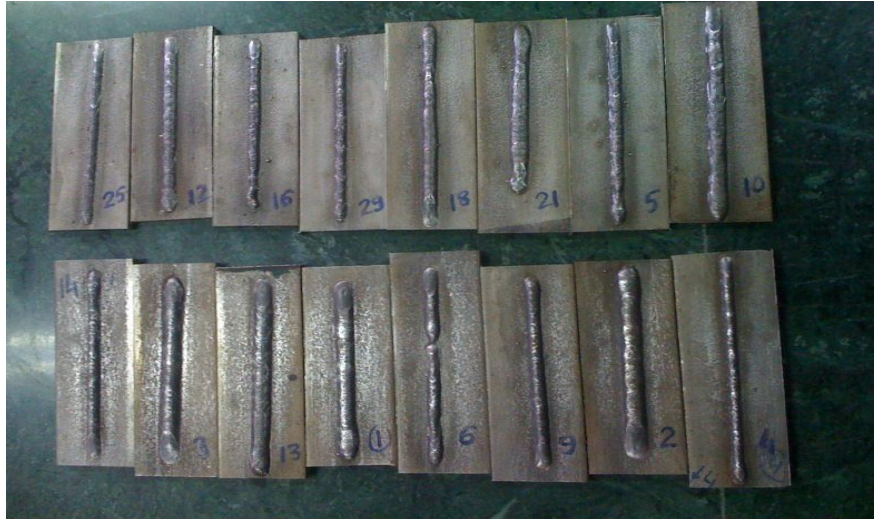
Figure: 3.3 welded plates

Table no: 3.3 Design parameters and their limits

PARAMETERSUSED	LEVELS				
	1 (-2)	2 (-1)	3 (0)	4 (1)	5 (2)
Plate thickness(mm)	3	6	8	12	15
Gas flow rate (lit/min.)	8	10	13	15	18
Current (A)	166	200	241	275	316
Travel speed (cm/min.)	27	32	37	42	47

Table no: 3.4 Recording of responses

Run order	Std. order	Sample No.	Input parameters (actual value)				Responses		
			T	G	S	I	Bead height	Bead width	Bead Penetration
1	03	1	6	15	32	200	3.16	7.44	2.11
2	24	2	8	13	37	136	3.35	10.22	2.45
3	16	3	12	15	42	275	3.56	8.14	1.96
4	29	4	8	13	37	241	3.1	8.85	2.48
5	04	5	12	15	32	200	2.86	6.95	1.46
6	21	6	8	13	27	241	3.17	8.08	1.62
7	01	7	6	10	32	200	3.63	6.98	1.63
8	10	8	8	10	32	275	3.3	6.59	1.63
9	05	9	6	10	42	200	3.71	8.16	2.15
10	28	10	8	13	37	241	3.58	10.02	2.18
11	08	11	12	15	42	200	3.74	6.55	1.72
12	11	12	6	15	32	275	2.93	6.92	1.86
13	23	13	8	13	37	166	3.51	9.33	2.13
14	22	14	8	13	47	241	3.5	10.18	1.89
15	02	15	12	10	32	200	3.78	7.56	1.98
16	26	16	8	13	37	241	3.13	6.92	2.04
17	12	17	12	15	32	275	3.59	7.76	1.99
18	30	18	8	13	37	241	3.16	8.69	2.26
19	15	19	6	15	42	275	3.26	10.12	2.27
20	18	20	15	13	37	241	3.38	7.02	2.12
21	27	21	8	13	37	241	3.35	8.7	2.05
22	14	22	12	10	42	275	3.23	7.79	1.9
23	19	23	8	8	37	241	3.28	7.28	1.76
24	25	24	8	13	37	241	3.78	7.81	1.82

25	06	25	12	10	42	200	3.47	7.71	1.89
26	20	26	8	18	37	241	3.44	7.79	1.91
27	09	27	6	10	32	275	3.47	7.78	1.9
28	07	28	6	15	42	200	3.46	7.52	1.93
29	13	29	6	10	42	241	3.52	7.73	1.92
30	17	30	3	13	37	241	3.45	7.78	1.89

In given table 3.4 recording of response select optimum parameter with respect to Bead height, bead width, bead penetration i.e. recording response of optimum parameter and then experimental analysis of optimum parameter.

Table no: 3.5   Recording response of optimum parameter

Sample no	Input parameter (actual value)				Response		
	T	G	S	I	Bead height	Bead width	Bead penetration
2	8	13	37	136	3.35	10.22	2.45
4	8	13	37	241	3.1	8.85	2.48
15	12	10	32	200	3.78	7.56	1.19
24	8	13	37	241	3.78	7.81	1.82

3.2 SAMPLE PREPARATION FOR BEAD MEASUREMENT

This procedure of preparation of a specimen involves the method of preparing the samples cut out from the plates fit for viewing under a metallurgical microscope. The ultimate objective is to produce a flat, scratch free, mirror like surface. The steps involved in our specimen preparation are as follows

a) Sampling: – The choice of a sample for microscopic study may be very important. If a failure is to be investigated, the sample should be chosen as close as possible to the area of failure and should be compared with one taken from the normal section. If the material is soft as non-ferrous metals and alloys and non-heat treated steels, the section may be obtained by manual hack sawing. If the material is hard, the section may be obtained by use of an abrasive cutoff wheel. In our case it was stainless steel hence used grinding wheel for cutting the samples.

b) Rough grinding: – Whenever possible, the specimen should be of a size that is convenient to handle. Our sample is made flat by slowing moving it up and back across the surface of a flat smooth file. Specimen is made rough ground on a belt sander, with the specimen kept cool by frequent dropping in water during grinding operation. The rough grinding is continued until the surface is flat and free of nicks, burrs, etc., and all scratches due to the hacksaw or cutoff wheel are no longer visible.

c) Intermediate polishing or grinding: - Grinding is done using rotating discs covered with silicon carbide paper and water. There are a number of grades of paper, with 180,240, 400, 1000, grains of silicon carbide per square inch. 180 grades therefore represent the coarsest particles and this is the grade to begin the grinding operation. Always use light pressure applied at the center of the sample. Continue grinding until all the blemishes have been removed, the sample surface is flat, and all the scratches are in a single orientation. Wash the sample in water and move to the next grade, orienting the scratches from the previous grade normal to the rotation direction. This makes it easy to see when the coarser scratches have all been removed. After the final grinding operation on 1000 paper, the sample is washed

in water followed by acetone and dried before moving to the polishers.

d) Fine polishing: - The polishers consist of rotating discs covered with soft cloth impregnated with diamond particles (1 and 0.5 micron size) and an oily lubricant. It began with the 1 micron grade and polishing continued until the grinding scratches have been removed. It is of vital importance that the sample is thoroughly cleaned using soapy water, followed by acetone, and dried before moving onto the final 0.5 micron stage. A properly polished sample showed only the nonmetallic inclusions and will be scratch free.
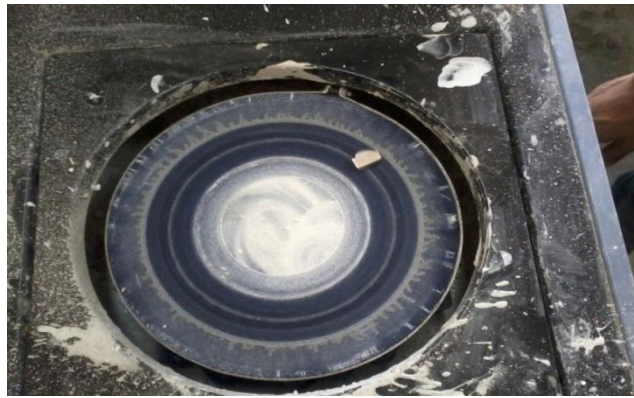
Figure: 3.4 Polishing machine.

e) Etching: - The purpose of etching is two-fold. Grinding and polishing operations produce a highly deformed, thin layer on the surface which is removed chemically during etching. Secondly, the etchant attacks the surface with preference for those sites with the highest energy, leading to surface relief which allows different crystal orientations, grain boundaries, precipitates, phases and defects to be distinguished in reflected light microscopy. There are many tried and tested etchants available but there are mandatory safety issues associated with the preparation and use of all of these. The selection of the appropriate etching reagent is determined by the metal or alloy and the specific structure desired for viewing. In this case I used ferric chloride and hydrochloric acid etching reagent. Its composition is ferric chloride (5g), hydrochloric acid (50ml), and water (10ml). And in this case the etching time is a few seconds to 1 min.

Figure: 3.5 samples after etching
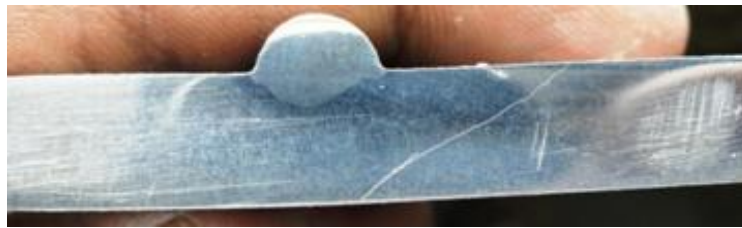
Figure: 3.6 bead geometry after etching

3.2.1 USING BAKELITE PRESS

For measurement of micro hardness sample will be flatness. To become flatness we use Automatic mounting press with Bakelite powder. This document provides a step-by-step procedure for mounting a specimen using the Buehler Simplimet 100 automatic specimen mounting press. General familiarity with the objectives and methods of mounting metallographic specimens is assumed. Even so, you should have a experienced person show you how to use this press.

1. Rough grind the metal specimen with 400 grit emery paper to flatness on the face to be investigated.

2. Clean die (piston, cylinder and bottom plug) for smooth operation.

3. Place specimen on bottom plug, face down.

4. Place cylinder over bottom plug and fill with Bakelite powder 1/2 to 2/3 to top.

5. Insert piston into cylinder, flat end down, and place heating element around die.

6. Apply 2800 psi cold, Plug in heater. Maintain at 2800 psi while heating by pumping as needed. When melted (no further drop in pressure), heat for 1 minutes and then cool for 3 minute by raising heater and using cooling fins.

7. Maintain pressure to about 2800 psi, release remaining pressure and press mold out of die.

8. Clean die. Thickness of the mount should be sufficient to enable the operator to hold the sample firmly during grinding, but if the mount is too thick, i.e. the powder is too much, it may not be focused very well in the microscope. On the other hand, if too little powder is used; it will cause a lot of problems while using the microscope and especially the hardness tester.

Figure: 3.7 Simplimet 100 Automatic Mounting Press.

Figure 3.8 Heat time and cool time of Automatic Mounting press.

Figure 3.9 sample prepare using automatic mounting press.

The Simplimet 3 is an automatic electro-hydraulic specimen mounting press. To mount a specimen the operator simply loads the press, starts the automatic molding sequence and pre-heating for some time and then heating for 1 minute after complete heating time then cool time start for 3 minute returns 5 to 10 minutes later to remove a cool mounted sample. The essential specifications of the Simplimet 3 include a maximum 200°C molding temperature which can be specified in 10°C steps, 0 to 4400 psi mounting pressure in 10 psi steps, 1 second to 30 minute molding time and a 100 psi pre-load.

CHAPTER 4

RESULT AND DISCUSSION

4.1 METALLURGICAL ANALYSIS

To carry out the metallurgical studies, specimens were cut in the transverse direction from the welded plates. After that, the specimens were polished with progressively finer grades of emery paper. After that wet polishing of the specimen was done; followed by etching with ferric chloride and hydrochloric acid etching reagent. Its composition is ferric chloride (5g), hydrochloric acid (50ml), and water (10ml). Micro structural studies were carried out on the weld zone, Heat Affected Zone and the Base metal, after preparing the specimens. The variation of micro hardness along the weld bead in horizontal direction was also determined.

4.1.1 MICRO STRUCTURAL ANALYSIS

Microstructure is defined as the structure of a prepared surface or thin foil of material as revealed by a microscope above 25× magnification. The microstructure of a material can strongly influence physical properties such as strength, toughness, ductility, hardness, corrosion resistance, high/low temperature behavior, wear resistance, and so on, which in turn govern the application of these materials in industrial practice. The micro structural features of a given material may vary greatly when observed at different length scales. For this reason, it is crucial to consider the length scale of the observations when describing the microstructure of a material. To study the Microstructure Olympus GX 41 microscope was used in conjunction with META-Lite Software.

Figure 4.1 Olympus GX 41microscope

In Olympus GX41 microscope show microstructure test report on figure 4.2 according to Graphite Flake Analysis ASTMA247-67.There is different type of Flake name A, B, C, D, E and the total Flake size was 5 to 6.

MICROSTRUCTURE TEST REPORT
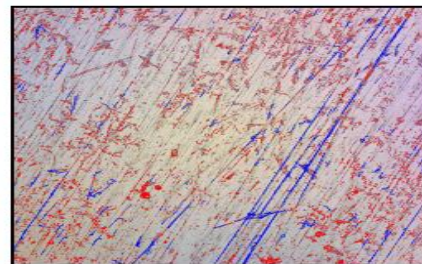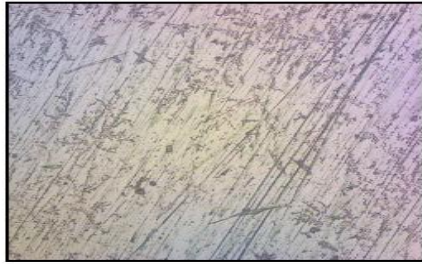
Graphite Flake Analysis ASTMA247-67

NAME	STATISTICS
Flake_A	2.9
Flake_B	0
Flake_C	0
Flake_D	0
Flake_E	0
Combined	97.1
Flake_Size	5 To 6

Figure 4.2 Micro structure test report

MICROSTRUCTURE TEST REPORT
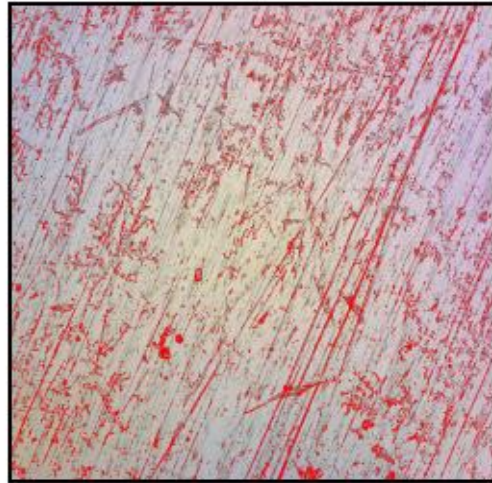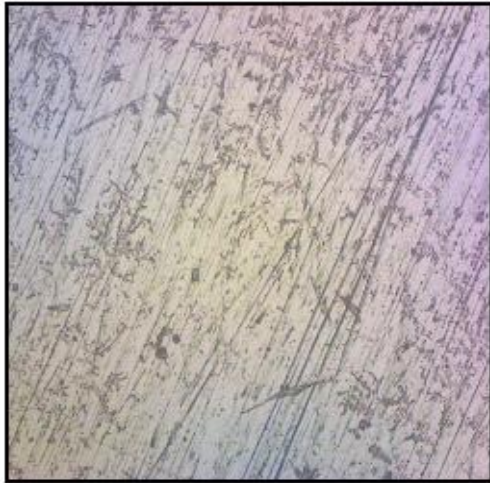
POROSITY ANALYSIS ASTM B 276

FIELD	TOTAL	POROSITY_PERCENTAGE	MAX_PERI	MIN_PERI	MAX_AREA	MIN_AREA
Field 1	6729	8.89	298.2462	1.1205	93.5283	0.0785
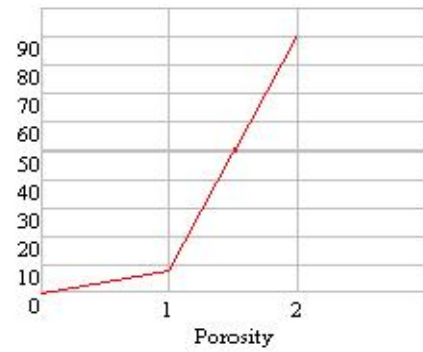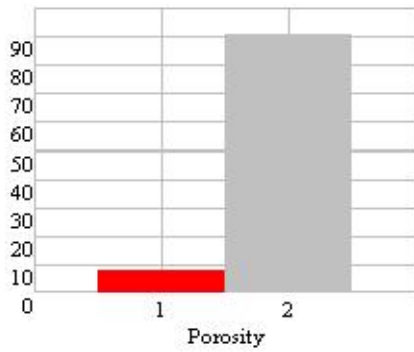
Figure: 4.3 Micro structure test report

In Olympus GX41 microscope show microstructure test report on figure 4.3 according to Porosity Analysis ASTM B276 total porosity percentage is 8.89%
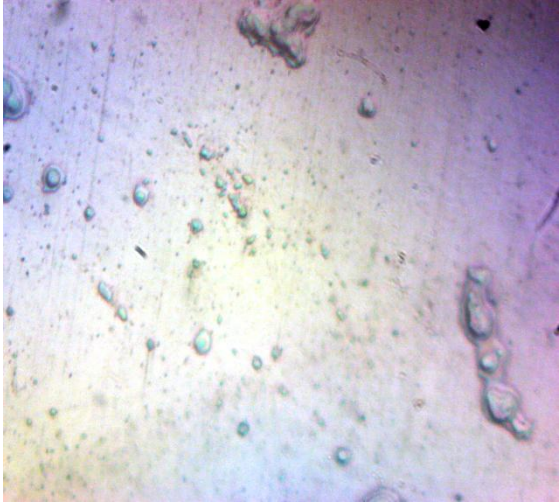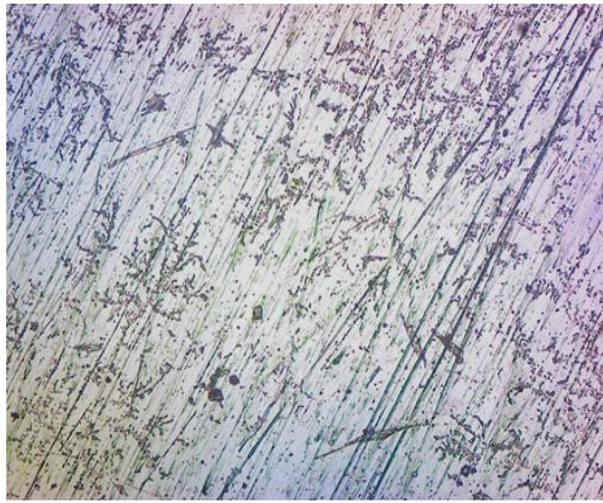
(a) Sample 2   (b) Sample 4

Figure: 4.4 Micro structure at magnification 100x.90 (a) Sample2 (b) Sample4
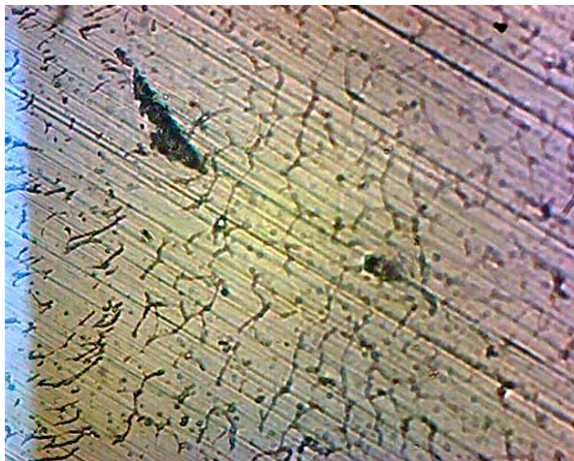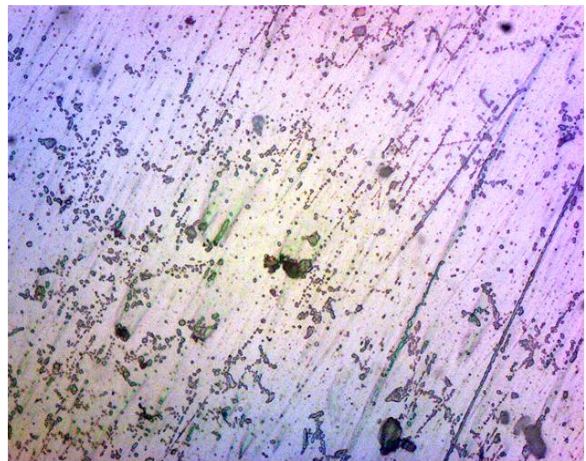
(c) Sample 15   (d) Sample 24

Figure: 4.5 Micro structure at magnification 50x.75 (a) Sample15 (b) Sample24

The microstructure is shown above. In the micro structure the inclusions and porosity were found. These inclusions and porosity may be due to carbon dioxide in the shielding gas composition. The size of pores and inclusions are small as current increases base material microstructure is presented Figure 4.4 and 4.5 Well-defined grain boundaries are shown. When the temperature is very high water disintegrates into H_2 and O_2 and as H_2 comes out it leaves large no of

fine holes on the surface of welded part .This defect is called pin hole porosity. Figure 4.4 (a) sample 2 Spatter occurs when the weld puddle expels molten metal and scatters it along the weld bead; this molten metal then cools and forms a solid mass on the work piece. Excessive spatter not only creates a poor weld appearance, but it can also lead to incomplete fusion in multiple welding pass applications

4.1.2 Micro hardness

Macro hardness testing, also commonly referred to as Knoop or Vickers testing, is also performed by pressing an indenter of specified geometry into the test surface. Unlike Rockwell testing, the Knops or Vickers test applies only a single test force. Knoop tests are mainly done at test forces from 10g to 1000g, Knoop tests are mainly known as micro hardness or Micro indentation tests and are best used in small test areas or on brittle materials as minimal material deformation occur on the short diagonal area. The Vickers diamond produces a square based pyramidal shape with a depth of indentation of about 1/7th of the diagonal length. The Vickers test has two distinct force ranges, micro (10g to 1000g) and macro (1kg to 100kg), to cover all testing requirements. The indenter is the same for both ranges therefore Vickers hardness values are continuous over the total range of hardness for metals (typically HV100 to HV1000). Vickers tests are mainly known as macro-indentation tests and are used on a wider variety of materials including case hardened, and steel components. Vickers indents are also less sensitive to surface conditions than the Knoop test. Variation of micro hardness was observed at the various points. To measure the Vickers micro hardness according to ASTME-384-89, Omnitech MVH Auto Micro Hardness tester (Figure 4.6) was used with 100 gram load and dwell time of 10 seconds.

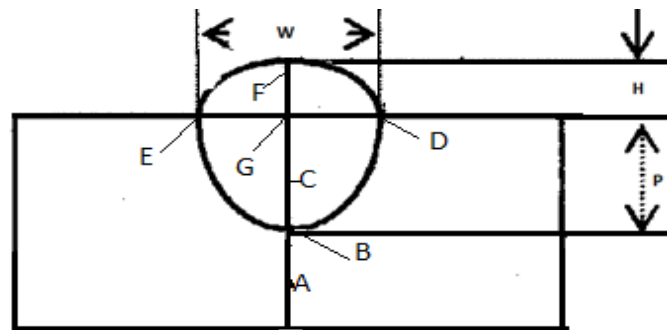Figure 4.6 Omnitech MVH Auto Micro Hardness tester

Figure 4.7 Varies points on bead to measure the micro hardness

The micro hardness values were calculated at various points. These points are different -2 regions, staring from point A to point G. The points are shown in figure 4.7.The values reported are for Vickers Micro hardness. A pyramidal diamond point is pressed into the polished surface of the test material with a known force, for a specified dwell time 10 sec, and the resulting indentation is measured using a microscope. The calculated value of micro hardness are shown table 4.1. The micro hardness (VHN) test was performed on the etched transverse cross-section of the laser–GMAW hybrid weld zone using a load of 1

kg, which was applied for duration of 20 s. seven measurements in each hybrid weld zone (base material across the weld toward its opposite side) were taken at regular intervals.

4.1.3 INSTRUCTIONS FOR MICRO HARDNESS TESTS

(1) All tests are started from the set point of A to G.

(2) The load should be applied in such a way that the direction of loading and the test surface are perpendicular to each other. If the sample surface is tilted after grinding or the amount of Bakelite powder used during the mounting procedure is insufficient, the measured hardness will be inaccurate.

(3) The load should be applied steadily to avoid overloading caused by the inertia of the weights.

 (4) The distance from center-to-center of indentations must be at least three indentation diameters so that the results of one indentation are not influenced by the deformation caused by the previous.

Table no: 4.1 Micro hardness of samples

Sample no	A	B	C	D	E	F	G
2	350	318	322	292	307	263	266
4	355	321	326	321	317	300	317
15	354	321	330	284	335	300	288
24	358	287	327	296	335	313	292
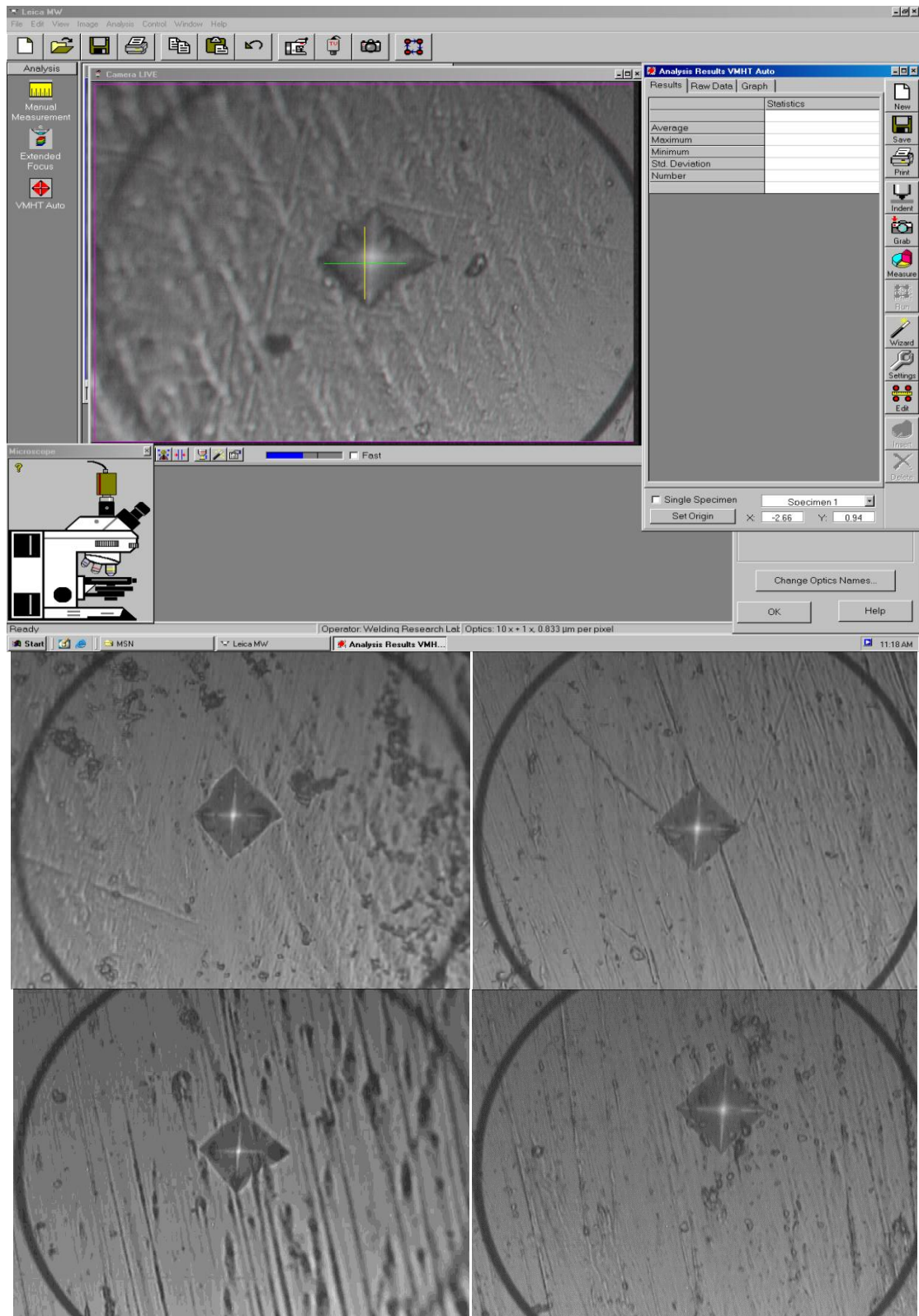
Figure: 4.8 Indentation of Sample 2, sample 4, Sample 15 and sample 24
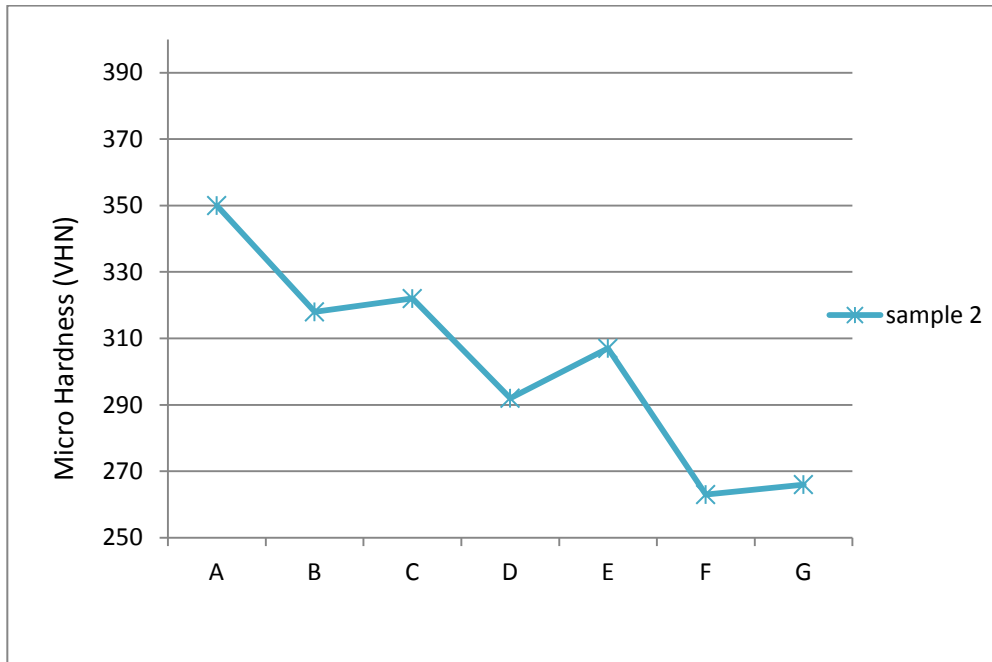
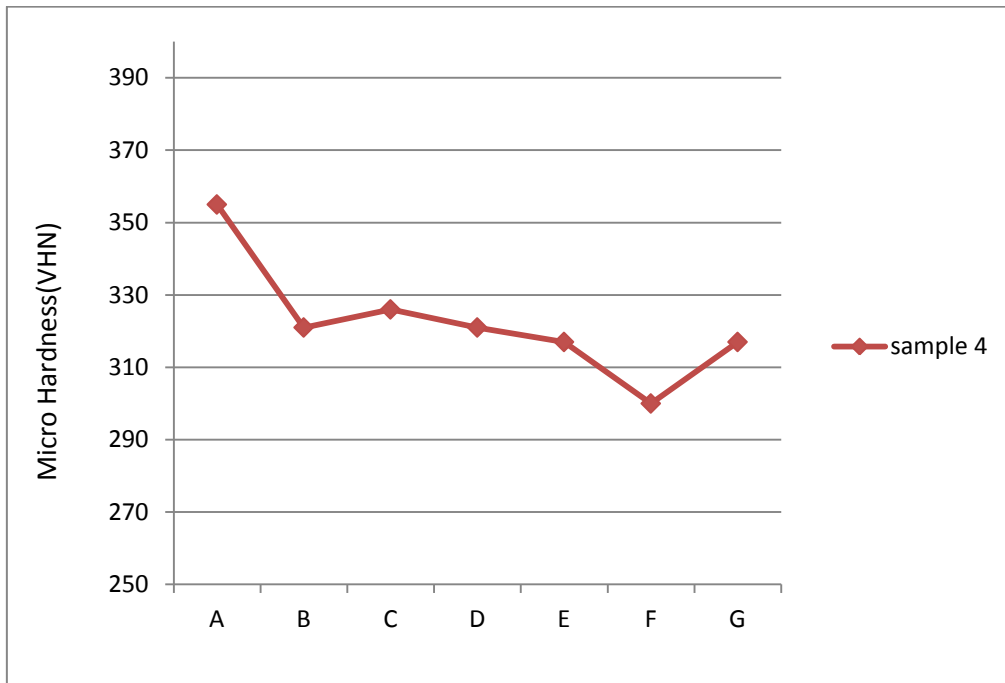Figure: 4.9 variation of micro hardness at various points on sample no 2

Figure: 4.10 variation of micro hardness at various points on sample no 4
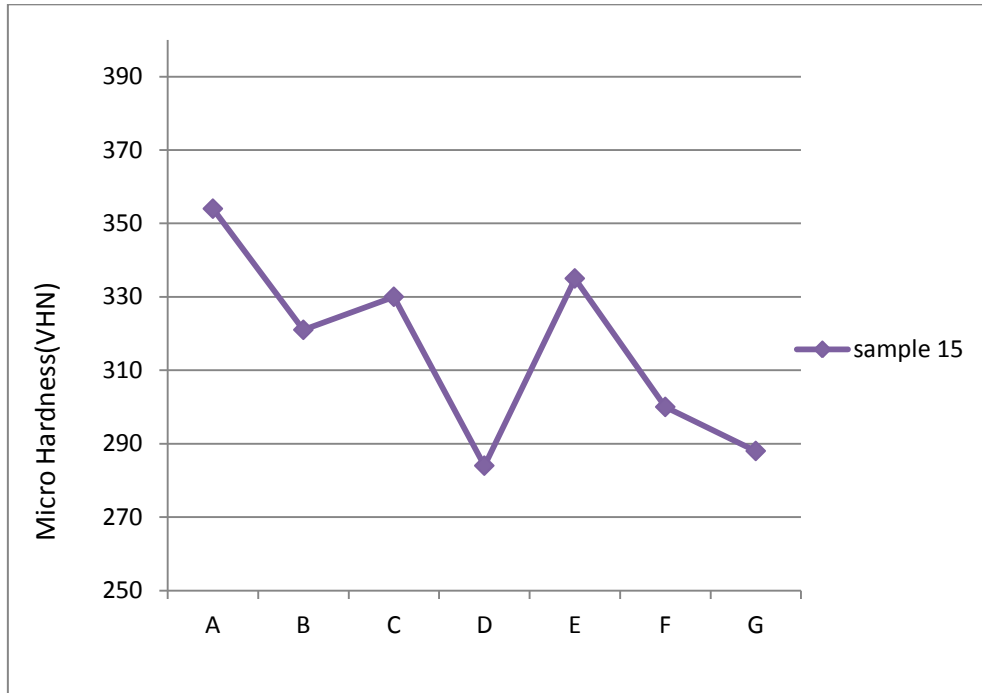
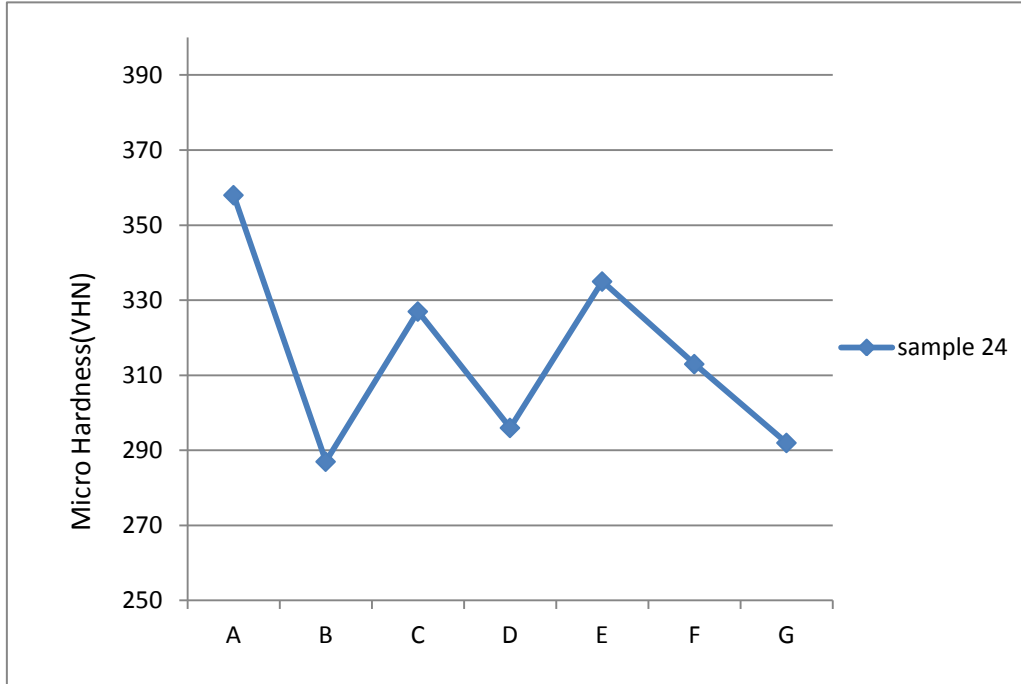Figure: 4.11 variation of micro hardness at various points on sample no 15

Figure: 4.12 variation of micro hardness at various points on sample no 24
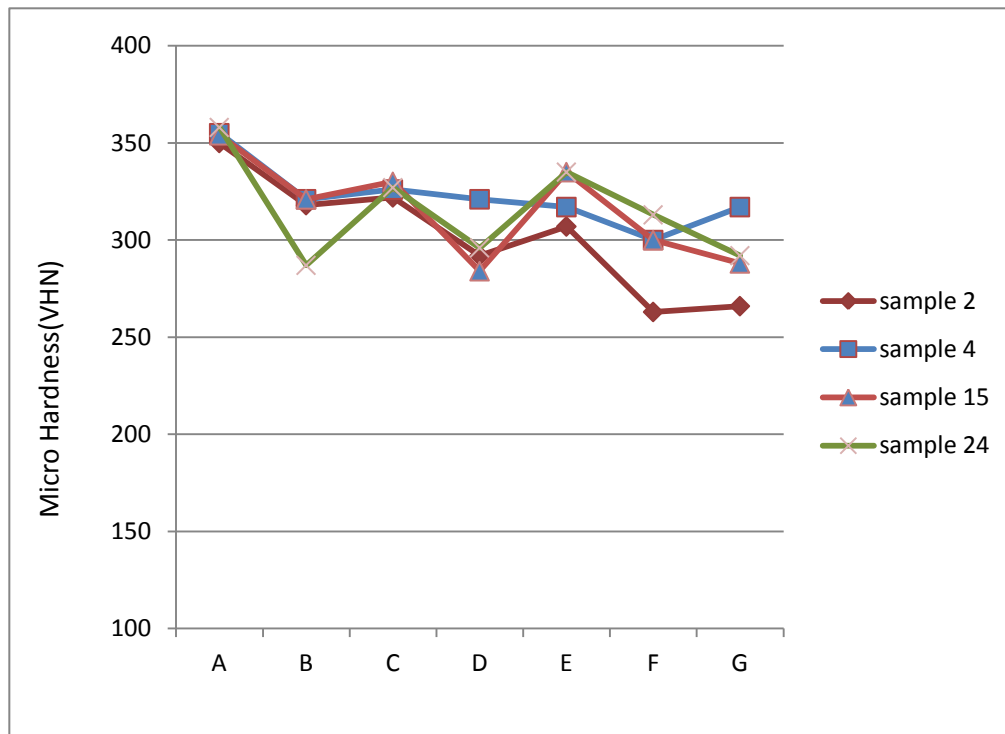
Figure: 4.13 Vickers Micro hardness at various points.

Micro hardness has been tested on micro hardness machine Omnitech MVH Auto Micro Hardness tester. The micro hardness values at different point are obtained. For base metal the micro hardness value is measured as 350VHN. The graphs are plotted between micro hardness and various points. From above table we see that the VHN value for the weld zone and the base metal are comparable while maximum hardness is observed at point A and E. These points are in the base metal. So the maximum micro hardness value is observed in base metalIt was observed that the hardness value is maximum for base metal and minimum in the HAZ region. It is also observed that the hardness values tested at different points in fusion zone is more than hardness value in HAZ region.

4.2 TENSILE TESTING

The tensile testing is carried out by applying longitudinal or axial load at a specific extension rate to a standard tensile specimen with known dimensions (gauge length and cross sectional area perpendicular to the load direction) till failure. The applied tensile load and extension are recorded during the test for the calculation of stress and strain. A range of universal standards provided by Professional societies such as American Society of Testing and Materials (ASTM), standard provides testing are selected based on preferential uses. Each standard may contain a variety of test standards suitable for different materials, dimensions and fabrication history. For instance, ASTM E8: is a standard test method for tension testing of metallic materials and ASTM is standard test methods of tension testing stainless steel.

Figure: 4.14 UTM setup

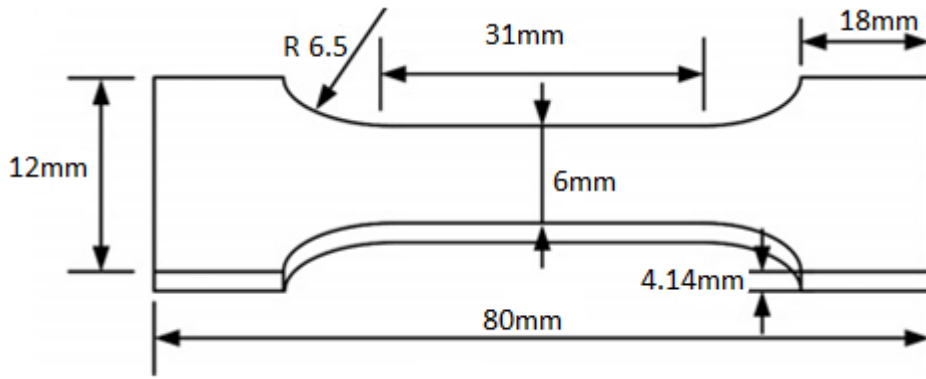Figure: 4.15 Fractured specimen after testing

Figure 4.16 specimen dimensions

A standard specimen is prepared in a square section along the gauge length as shown in figure4.16 depending on the standard used. Both ends of the specimens should have sufficient length and a surface condition such that they are firmly gripped during testing. The initial gauge length Lo is standardized (in several countries) and varies with the diameter (Do) or the cross-sectional area (Ao) of the specimen. The tensile properties of the welded joints at room temperature. The tensile strength of the joints is basically comparable to that of the base metal and the tensile ductility of the joints achieves 89.126% of the base metal. These processes should be employed after specimen machining in order to obtain the tensile properties results which include the actual specimen surface conditions.

Table no: 4.2 Tensile test results

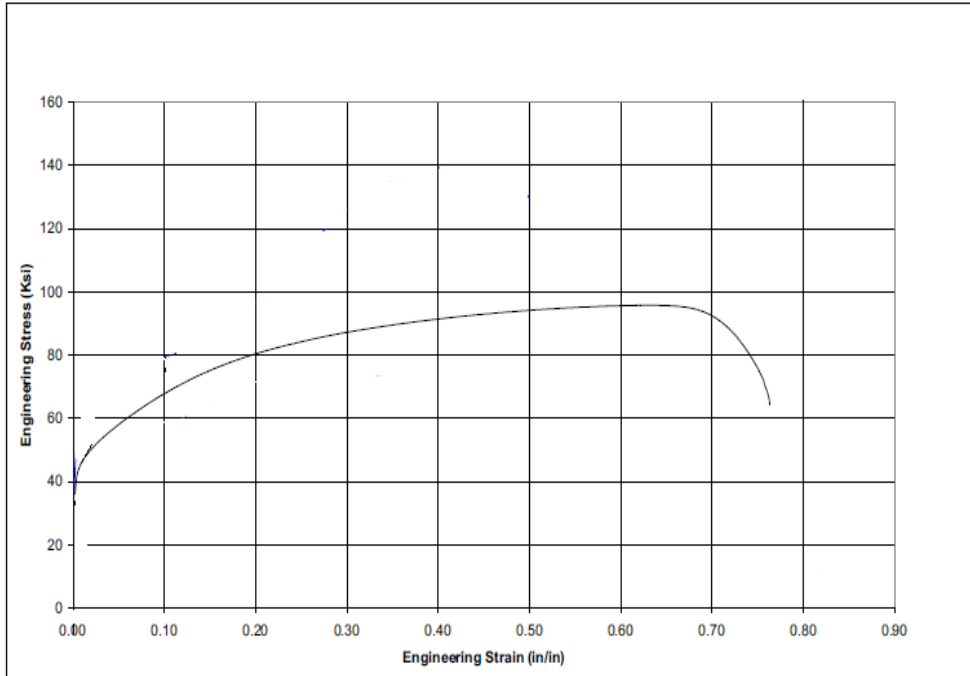|	Ultimate stress(MPa)	Ultimate strain	%Elongation	Yield strength(MPa)
304L Base Metal	659.828	0.642	76.3	275.75
304L Weld Metal	553.075	0.819	89.126	266.30

Figure: 4.17 Variation of engg stress vs engg strain base material
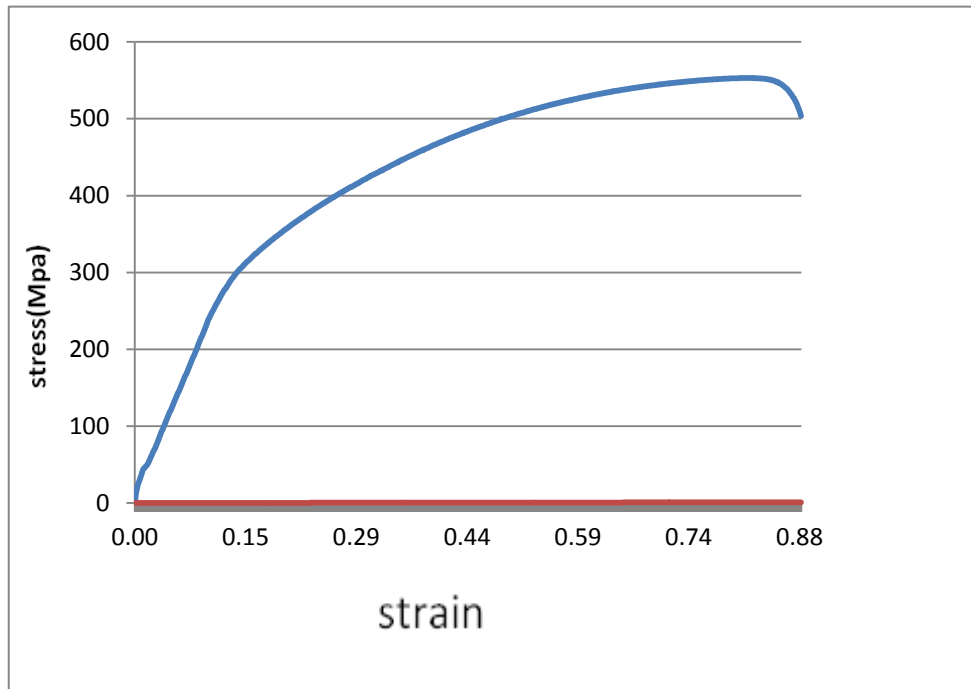

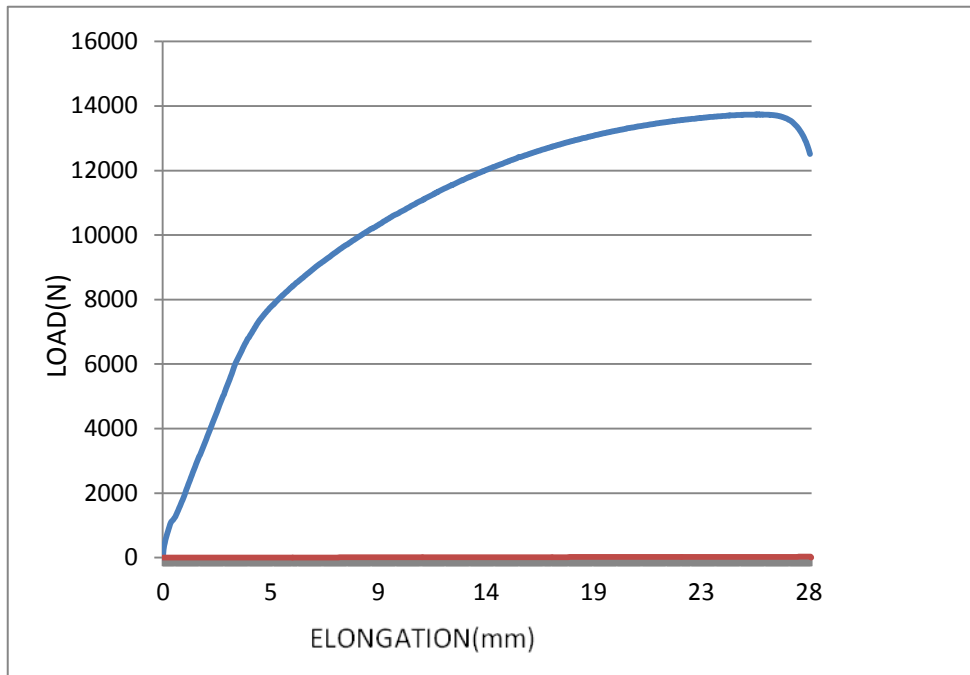Figure: 4.18 Variation of engg stress vs engg strain for welded specimen

Figure: 4.19 Variation of load vs. elongation for welded specimen

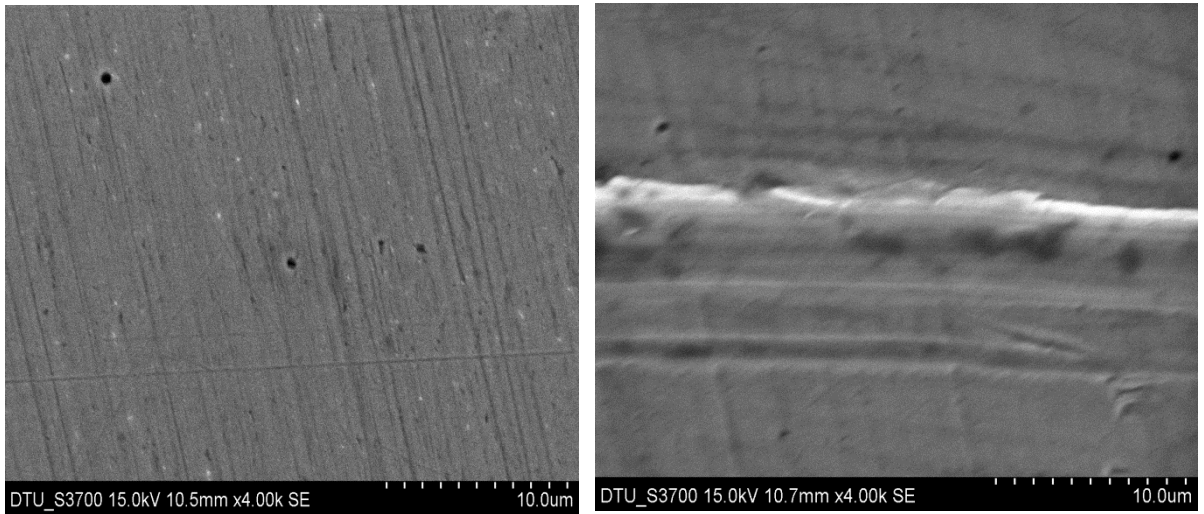## 4.3 Scanning Electron Microscope (SEM)

The SEM instrument is made up of two main components, the electronic console and the electron column. The electronic console provides control knobs and switches that allow for instrument adjustments such as filament current, accelerating voltage, focus, magnification, brightness and contrast. The art electron microscope that uses a computer system in conjunction with the electronic console making it unnecessary to have bulky console that houses control knobs, CRTs, and an image capture device. All of the primary controls are accessed through the computer system using the mouse and keyboard. The user need only be familiar with the GUI or software that controls the instrument rather than control knobs and switches typically found on older style scanning electron microscopes. The image that is produced by the SEM is usually viewed on CRTs located on the electronic console but, instead with FEI the image can be seen on

the computer monitor. Images that are captured can be saved in digital format or printed directly.
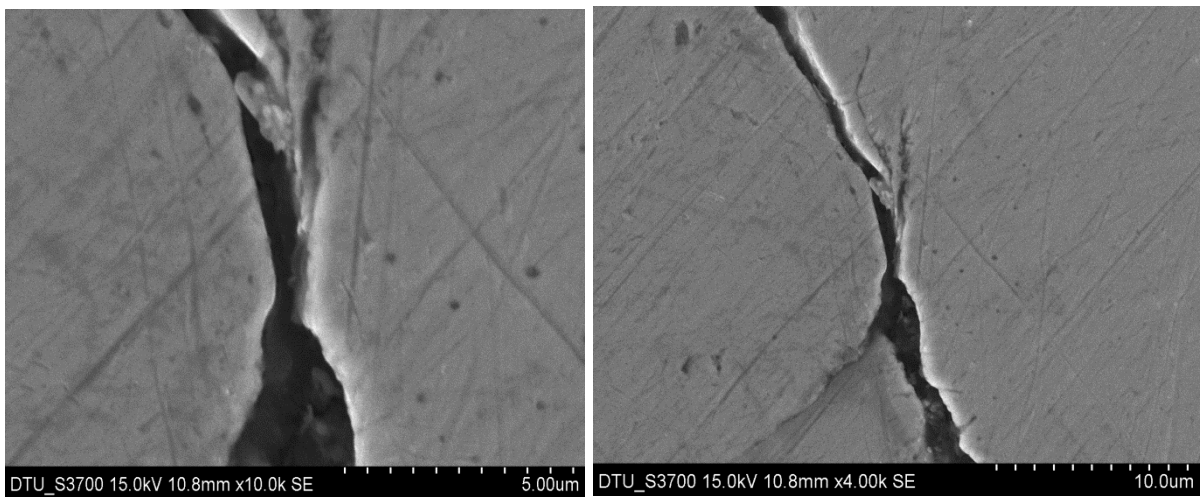

Figure: 4.20 Setup of Scanning Electron Microscope

The fracture surfaces of the weld metal specimens after polishing and then examined by the scanning electron microscope (SEM) equipped with energy dispersive spectroscope (EDS). The fractured surfaces of the welded specimens were analyzed using SEM. Figs.4.8-4.9 show the SEM fractographs of all welded specimens tested. Dimples of varying size and shape were observed in all the fractured surfaces which indicate that major fracturing mechanism was ductile. From Fig.4.8 sample 2 it is observed that fractured surface of the specimen porosity at bead geometry and a large population of small and shallow dimples. From fig 4.8 sample 4 it also observed that fracture surface at the weld bead and base metal boundary. From fig 4.9 sample 15 It is also observed that small dimples are surrounded by the large ones in all the specimens and a small quantity of tearing ridge is also present. A similar fractograph observation has been seen in the sample no 4 of welded specimen.
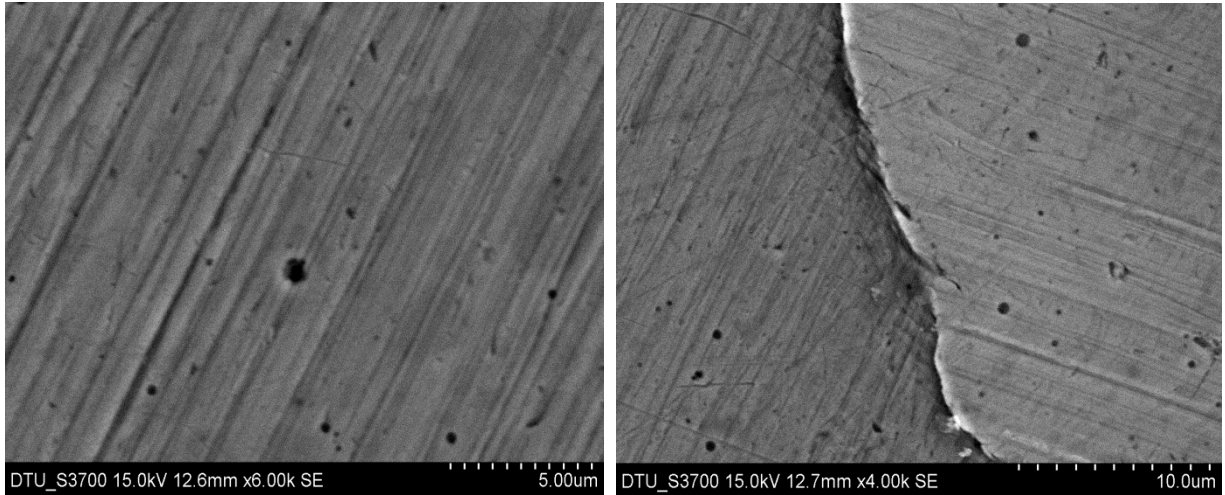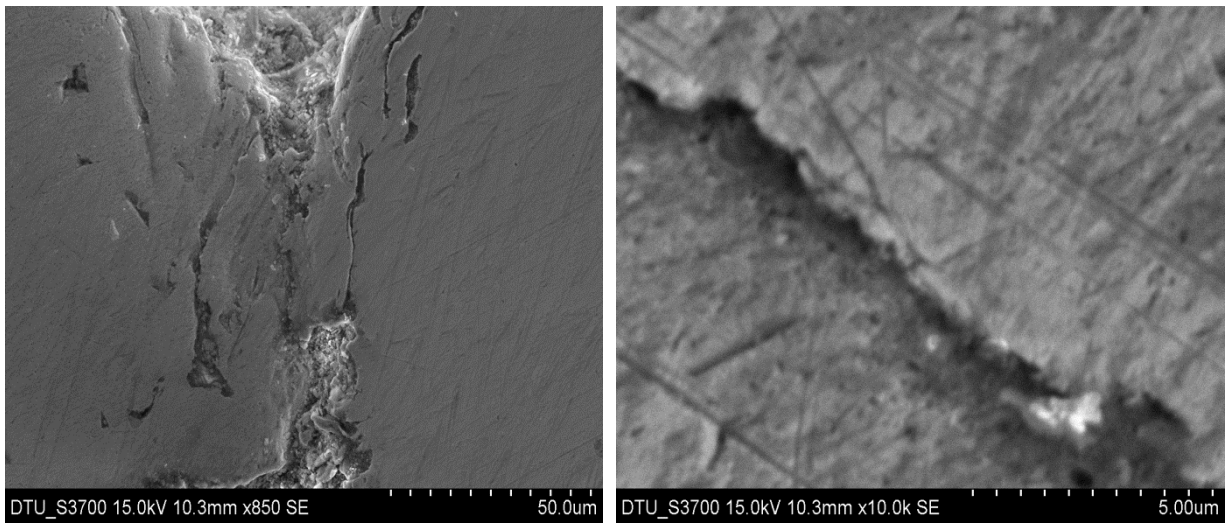
(a) Sample no 2

(b) Sample no 4

Figure: 4.21 SEM Micrograph of welded sample no 2 and 4

The observation of the microstructure of the fusion zone at higher magnification at 6000and 5.00 um and 4000 and 10 um in sample no 15 with scanning electron microscope showed very fine particles uniformly dispersed. . A similar fractograph observation has been seen in the sample no 24 of welded specimen.


(c)Sample 15

(d)Sample 24

Figure 4.22 SEM Micrograph of welded sample no 15 and 24

4.4 Energy Dispersive Spectroscopy (EDS)

Energy Dispersive Spectroscopy (EDS) allows one to identify what those particular elements are and their relative proportions (Atomic % for example). Initial EDS analysis usually involves the generation of an X-ray spectrum from the entire scan area of the SEM. Below is a secondary electron image of a polished geological specimen and the corresponding X-ray spectra that was generated from the entire scan area. The Y-axis shows the counts (number of X-rays received and processed by the detector) and the X-axis shows the energy level of those counts. The EDS software we have, "Noran System Six" (NSS), is quite good at associating the energy level of the X-rays with the elements and shell levels that generated them.
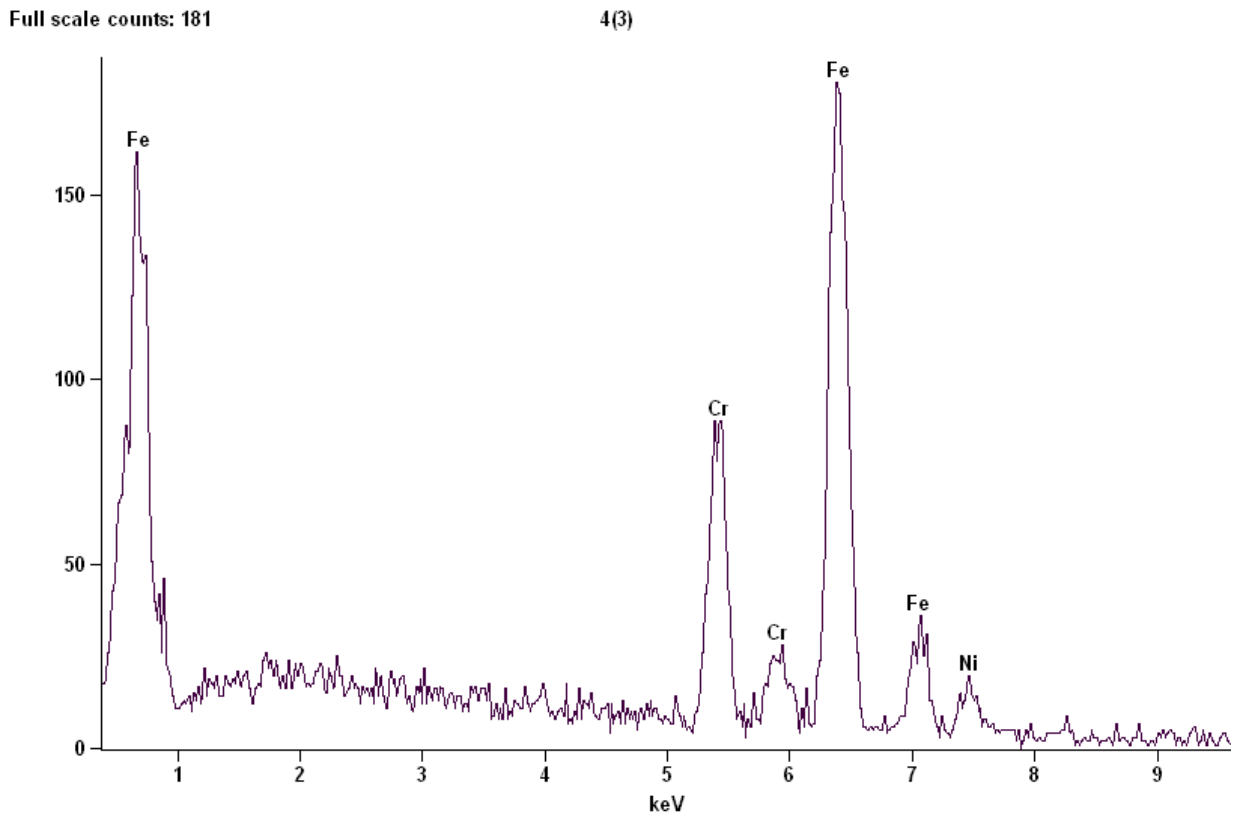

Acc. Voltage: 15.0 kV Take Off Angle: 41.8 deg.

Figure: 4.23 EDS Analysis welded specimen Sample 2
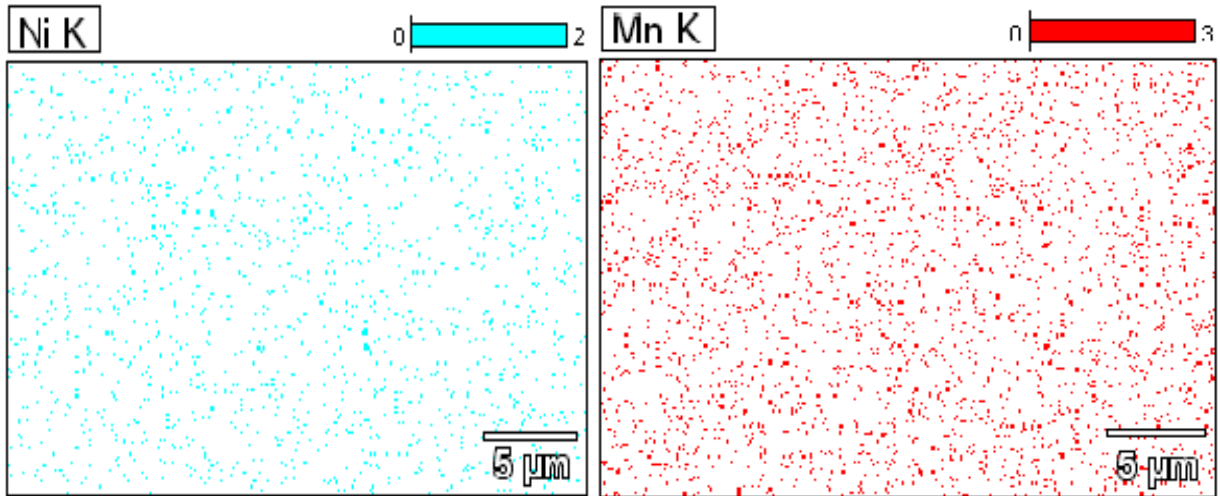
Table no: 4.3 Elemental compositions of sample 2

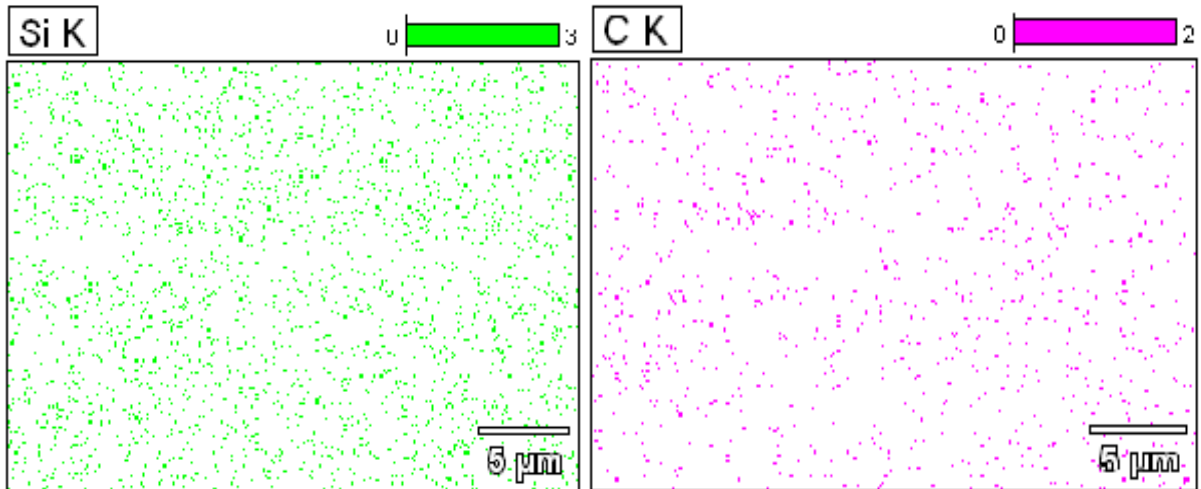| Element Line	Net Counts	Int. Cps/nA	Weight %	Weight % Error	Atom %	Atom % Error	Formula	Standard Name
Cr K	1652	0.001	19.78	+/- 0.97	21.02	+/- 1.03	Cr	
Cr L	1059	0.000	---	---	---	---		
Fe K	3563	0.001	71.95	+/- 2.42	71.19	+/- 2.40	Fe	
Fe L	2339	0.001	---	---	---	---		
Ni K	252	0.000	8.27	+/- 1.12	7.78	+/- 1.05	Ni	
Ni L	387	0.000	---	---	---	---		
Total			100.00		100.00			
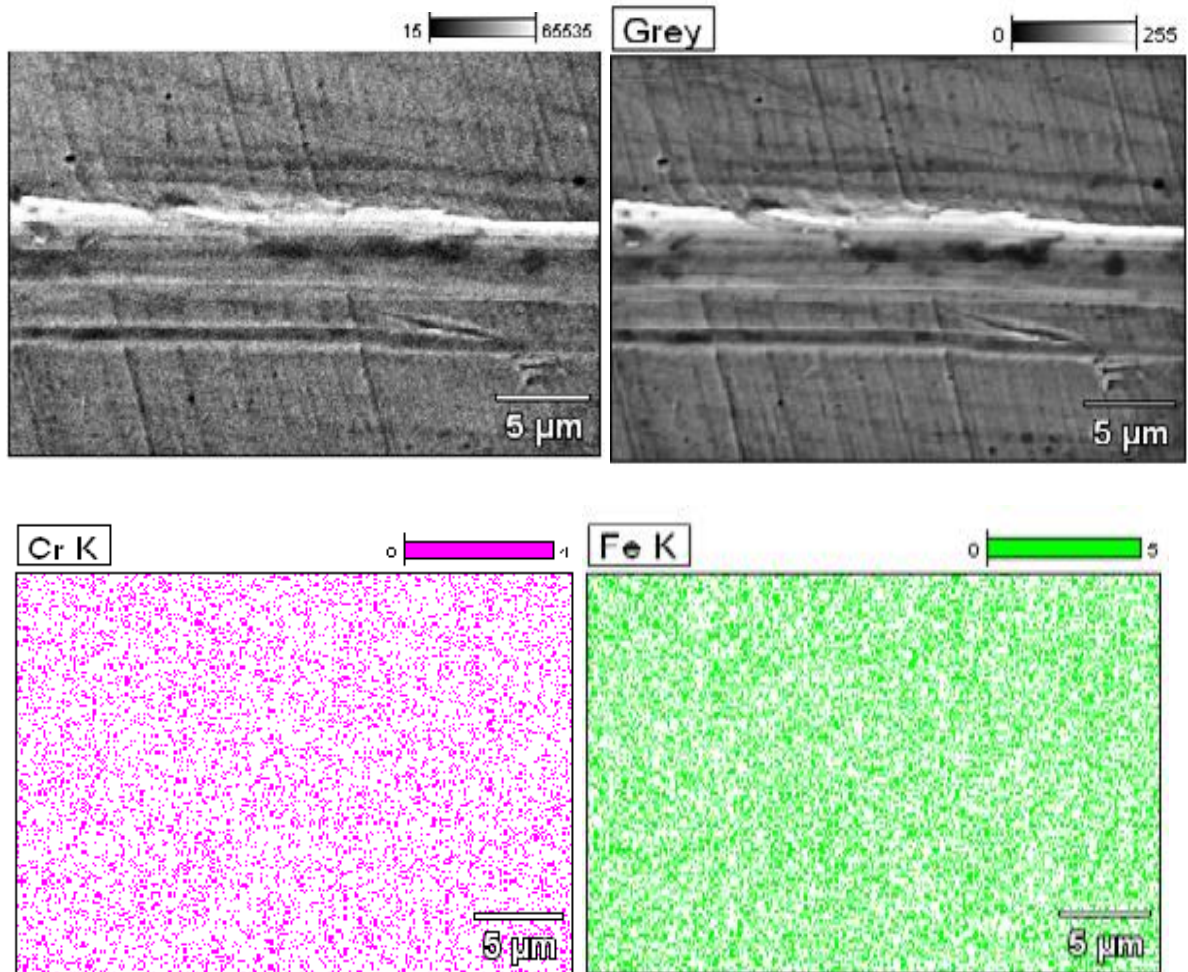
Data Type: Counts   Mag: 4000   Acc. Voltage: 15.0 kV

Figure: 4.24 Elemental compositions Sample 2

The results of EDS analysis presented in 4.24 and 4.25 shows that the inclusion particle mainly composed of Fe, Cr, Mn, Si, C elements. During welding, the shielding gas interacts with the weld pool and the addition of CO_2 and or O_2 in argon causes oxidation, which results in some losses of alloy constituents and produces inclusions in the weld.

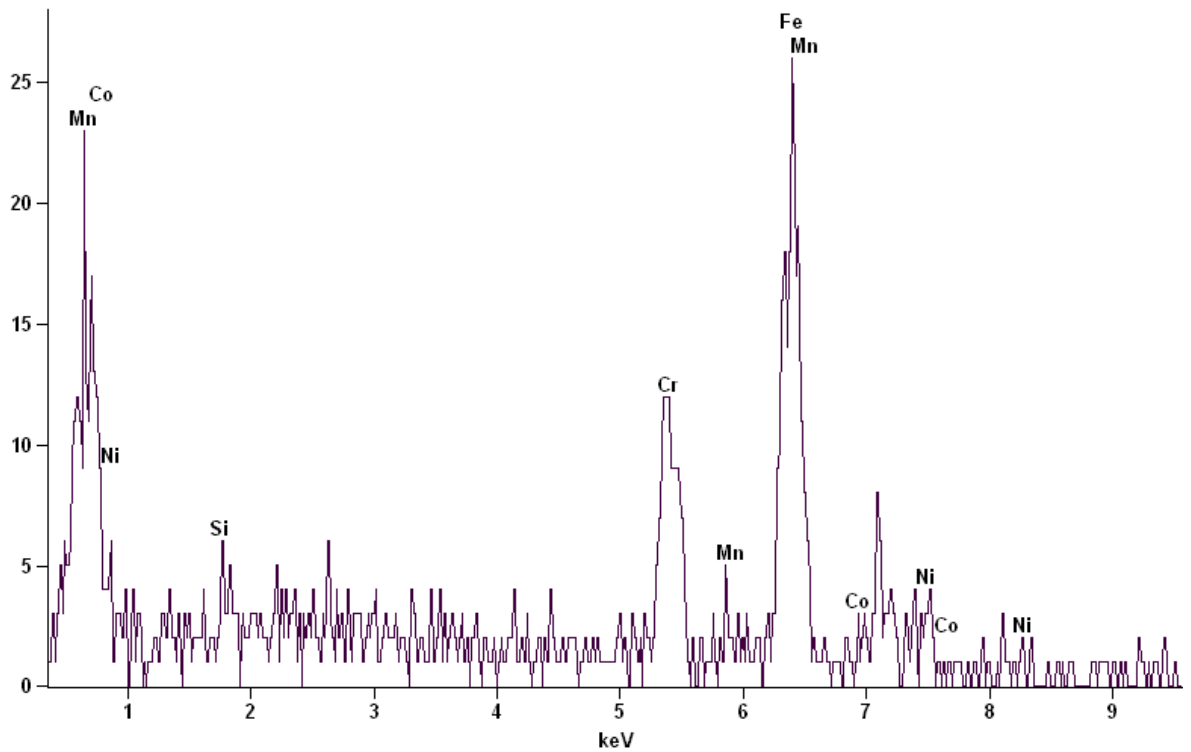Data Type: Counts   Mag: 4000   Acc. Voltage: 15.0 kV

Data Type: Counts Mag: 4000   Acc. Voltage: 15.0 kV

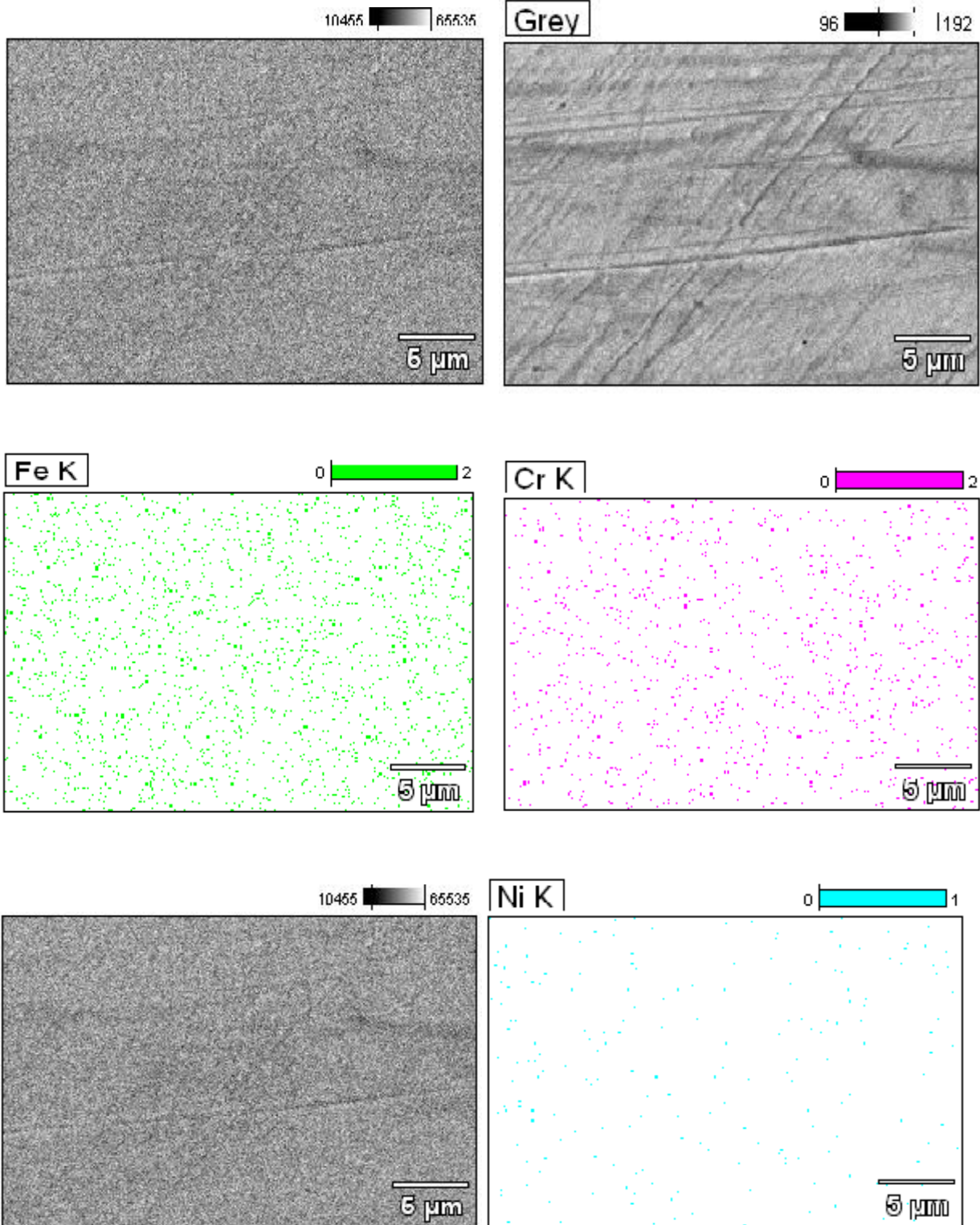Figure: 4.25 Elemental compositions Sample 2

Acc. Voltage: 15.0 kV Take Off Angle: 42.6 deg.

Table no: 4.4 Elemental compositions of sample 4

Element Line	Net Counts	Int. Cps/nA	Weight %	Weight % Error	Atom %	Atom % Error	Formula	Standard Name
C K	0	0.000	0.00	---	0.00	+/- 0.00	C	
Si K	8	0.000	0.35	+/- 0.39	0.68	+/- 0.77	Si	
Si L	0	0.000	---	---	---	---		
Cr K	206	0.000	21.86	+/- 3.08	23.12	+/- 3.25	Cr	
Cr L	48	0.000	---	---	---	---		
Mn K	0	0.000	0.00	---	0.00	+/- 0.00	Mn	
Mn L	65	0.000	---	---	---	---		
Fe K	389	0.000	69.00	+/- 5.32	67.95	+/- 5.24	Fe	
Fe L	173	0.000	---	---	---	---		
Co K	2	0.000	0.34	+/- 2.22	0.32	+/- 2.07	Co	
Co L	22	0.000	---	---	---	---		
Ni K	29	0.000	8.46	+/- 3.50	7.92	+/- 3.28	Ni	
Ni L	22	0.000	---	---	---	---		
Total			100.00		100.00			

Figure: 4.26 EDS Analysis welded specimen Sample 4
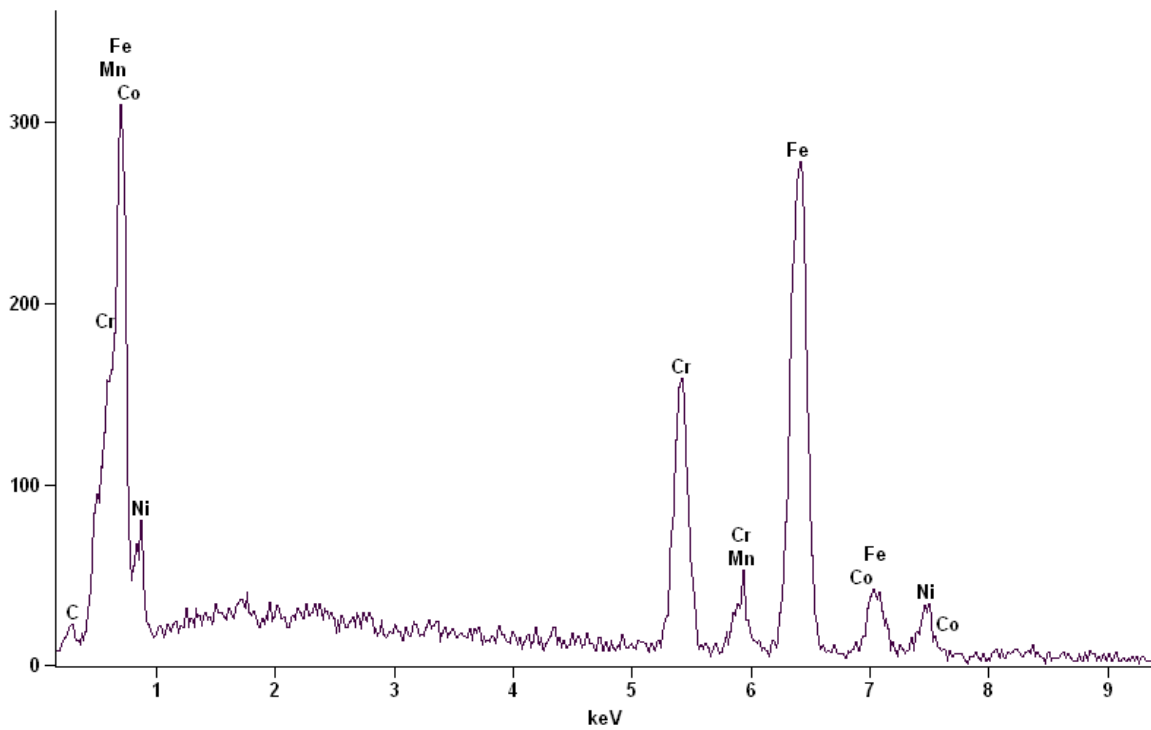
Data Type: Counts   Mag: 4000   Acc. Voltage: 15.0 kV

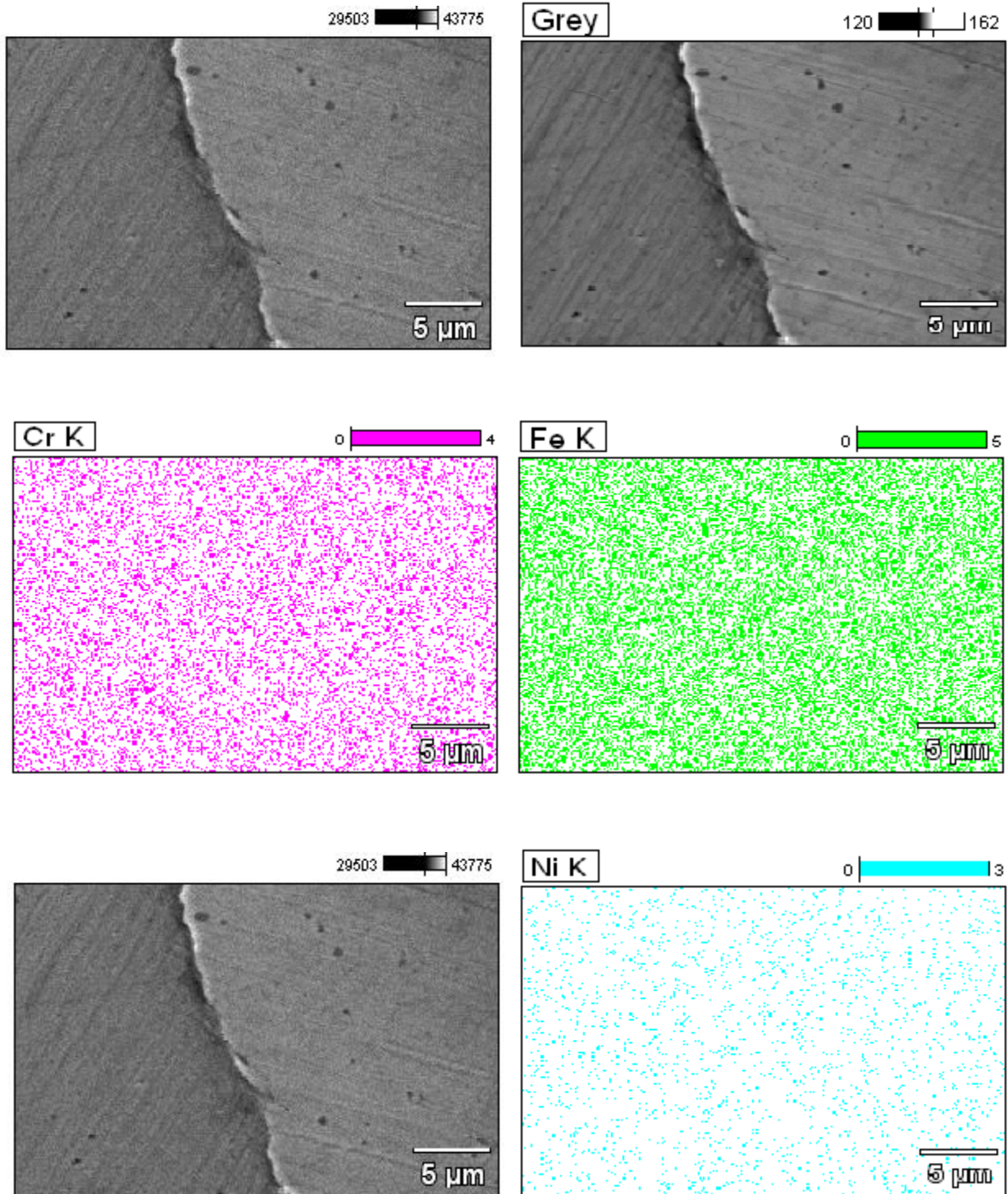Figure: 4.27 Elemental compositions Sample 4

Acc. Voltage: 15.0 kV Take Off Angle: 53.7 deg.

Table no: 4.5 Elemental compositions of sample 15

Element Line	Net Counts	Int. Cps/nA	Weight %	Weight % Error	Atom %	Atom % Error	Formula	Standard Name
C K	0	0.000	0.00	---	0.00	+/- 0.00	C	
Cr K	2248	0.001	19.39	+/- 0.76	20.62	+/- 0.81	Cr	
Cr L	1120	0.000	---	---	---	---		
Mn K	206	0.000	2.62	+/- 0.52	2.64	+/- 0.52	Mn	
Mn L	512	0.000	---	---	---	---		
Fe K	4675	0.001	67.80	+/- 1.81	67.14	+/- 1.80	Fe	
Fe L	3126	0.001	---	---	---	---		
Co K	20	0.000	0.37	+/- 0.75	0.35	+/- 0.70	Co	
Co L	175	0.000	---	---	---	---		
Ni K	419	0.000	9.82	+/- 0.87	9.25	+/- 0.82	Ni	
Ni L	527	0.000	---	---	---	---		
Total			100.00		100.00			

Figure: 4.28 EDS Analysis welded specimen Sample 15

Data Type: Counts   Mag: 4000   Acc. Voltage: 15.0 kV

Figure: 4.29 Elemental compositions Sample 15

Data Type: Counts   Mag: 4000   Acc. Voltage: 15.0 kV

Figure: 4.30 Element compositions Sample 15

15(4)

Acc. Voltage: 15.0 kV Take Off Angle: 37.7 deg.

Table no: 4.6 Elemental compositions of sample 24

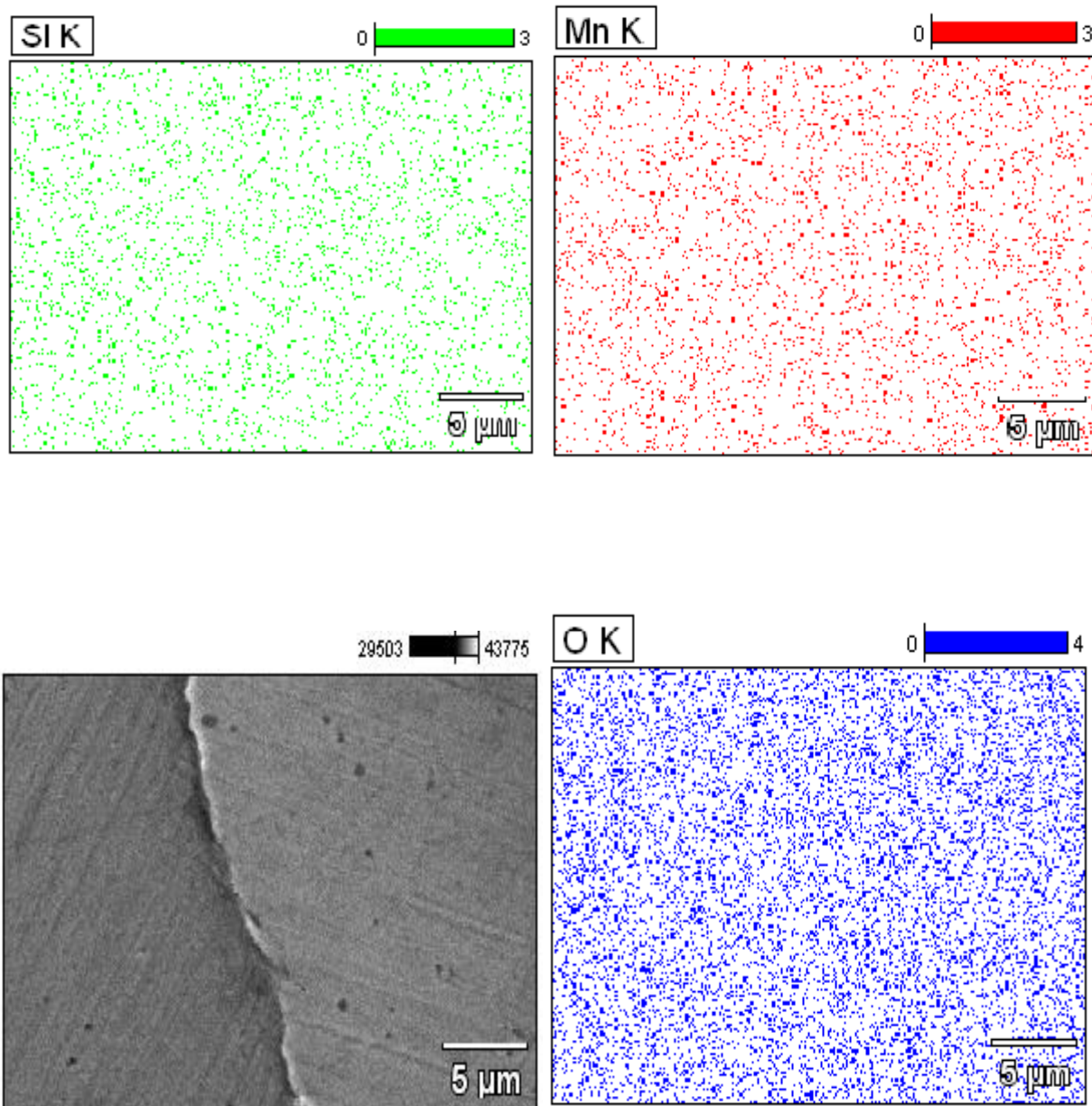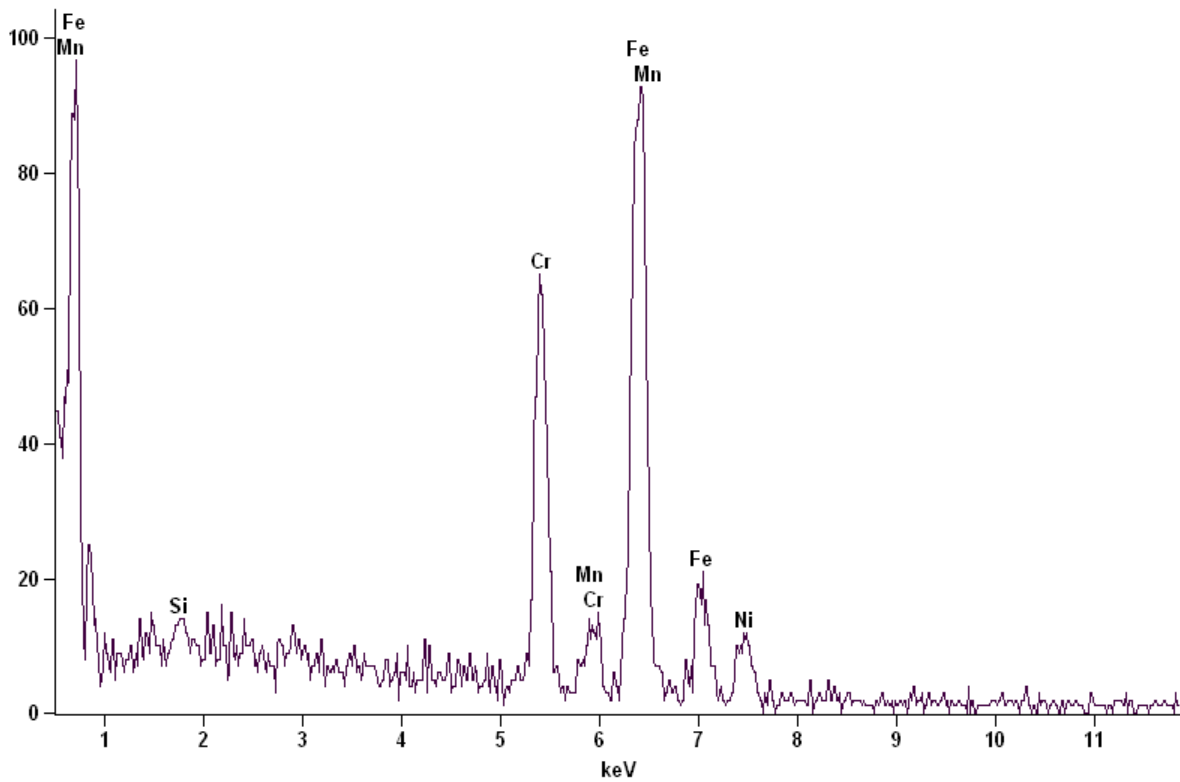| Element Line	Net Counts	Int. Cps/nA	Weight %	Weight % Error	Atom %	Atom % Error	Formula	Standard Name
C K	30	0.000	0.69	+/- 0.28	3.08	+/- 1.23	C	
Si K	51	0.000	0.51	+/- 0.16	0.98	+/- 0.31	Si	
Si L	0	0.000	---	---	---	---		
Cr K	906	0.000	20.96	+/- 0.86	21.63	+/- 0.88	Cr	
Cr L	429	0.000	---	---	---	---		
Mn K	38	0.000	1.28	+/- 0.84	1.25	+/- 0.83	Mn	
Mn L	39	0.000	---	---	---	---		
Fe K	1717	0.001	66.12	+/- 2.16	63.52	+/- 2.07	Fe	
Fe L	995	0.000	---	---	---	---		
Ni K	167	0.000	10.43	+/- 1.37	9.53	+/- 1.26	Ni	
Ni L	136	0.000	---	---	---	---		
Total			100.00		100.00			

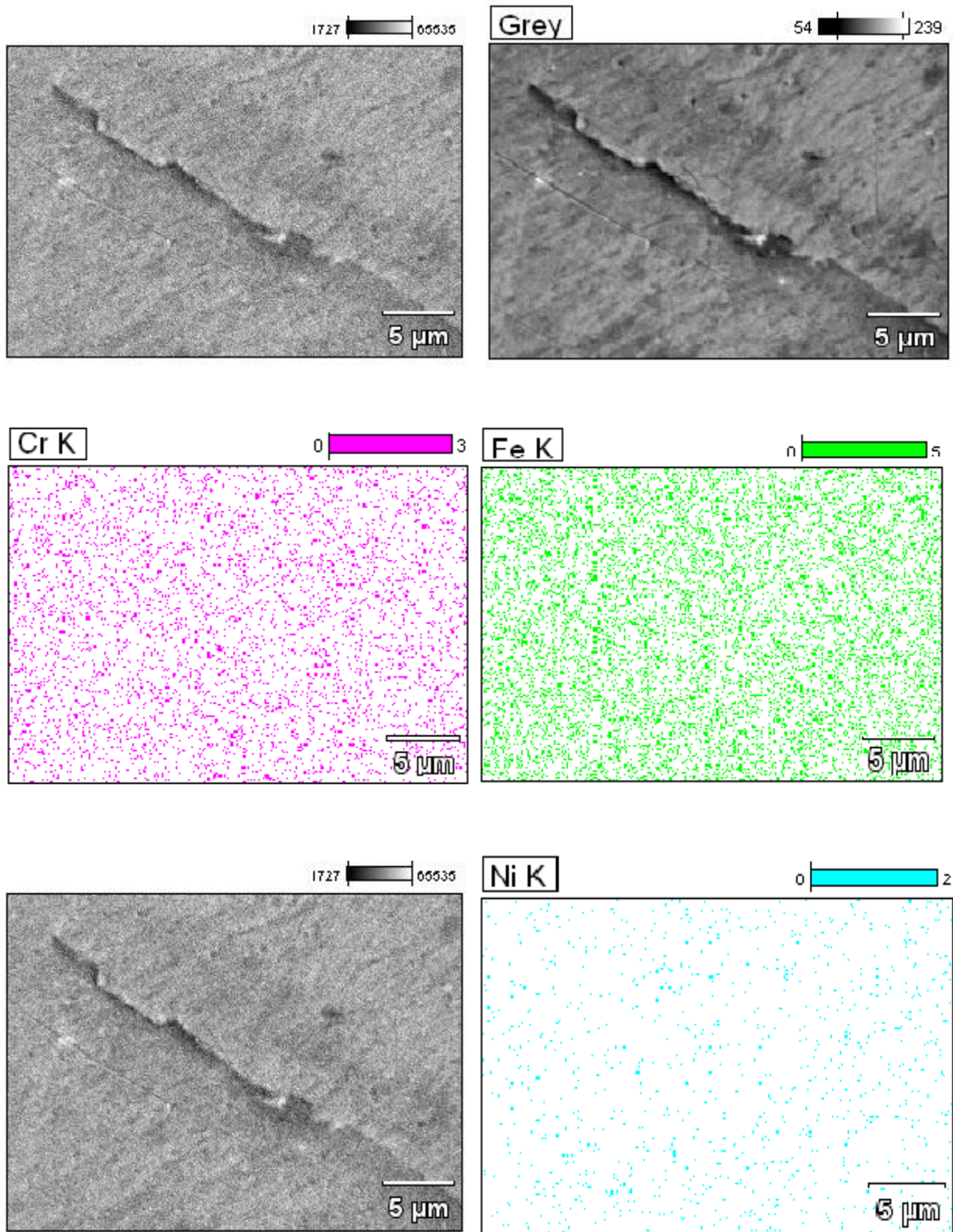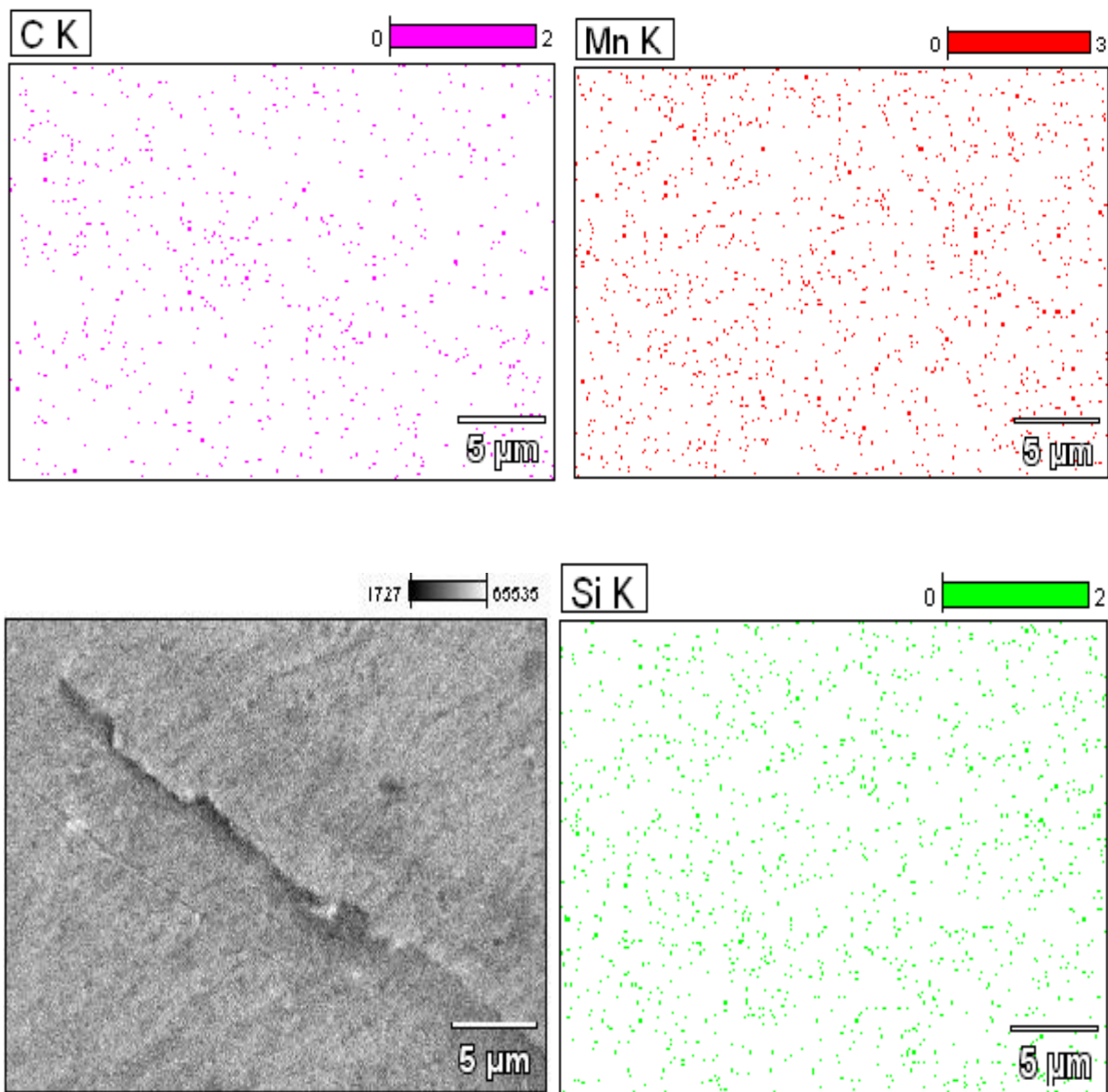Figure: 4.31 EDS Analysis welded specimen Sample 24

Figure: 4.32 Elemental compositions Sample 24

Data Type: Counts   Mag: 4000   Acc. Voltage: 15.0 kV

Figure: 4.33 Elemental compositions of Sample 24

4.5 X-RAY DIFFRACTION TECHNIQUE (XRD)

The purpose of this study was to investigate the metallurgical phases of 304L SS joints prepared by synergic MIG welding, using the X-ray diffraction technique (XRD), XRD analyses were performed at room temperature.

Figure: 4.34 Set up of x-ray diffraction

X-ray scattering techniques are a family of non-destructive analytical techniques which reveal information about the crystallographic structure, chemical composition, and physical properties of materials and thin films. These techniques are based on observing the scattered intensity of an X-ray beam hitting a sample as a function of incident and scattered angle, polarization, and wavelength or energy. XRD analysis is based on constructive interference of mochromatic x-rays and a crystalline sample. The x-rays are generated by a cathode ray tube, filtered to produce monochromatic radiation, collimated to concentrate, and directed toward the sample .the interaction of the incident rays with the sample produce

constructive interference and a diffracted ray when condition satisfy Bragg's law (n =2dsin). This law relates the wavelength of electromagnetic radiation to the diffraction angle and the lattice spacing in a crystalline sample.
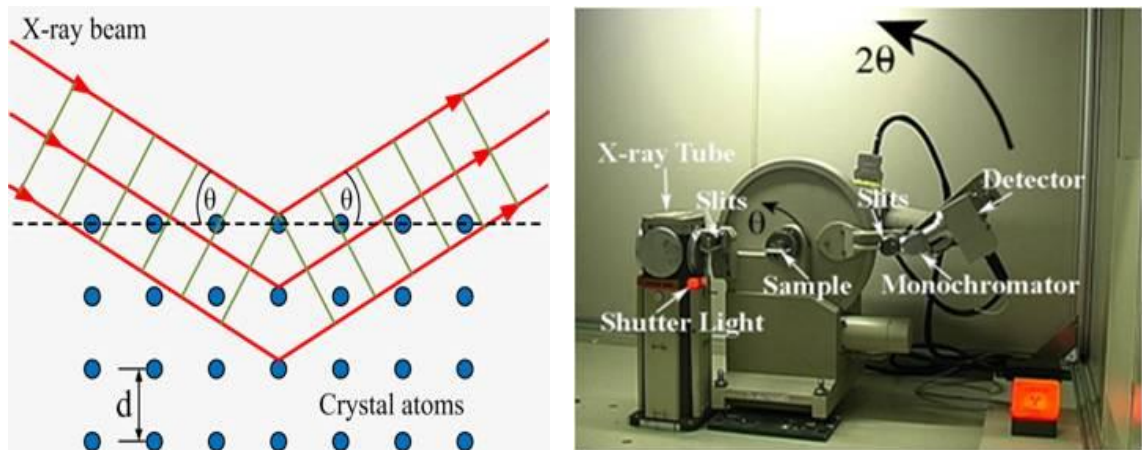

Figure: 4.35 principle of XRD

Although Bragg's law was used to explain the interference pattern of X-rays scattered by crystals, diffraction has been developed to study the structure of all states of matter with any beam, e.g., ions, electrons, neutrons, and protons, with a wavelength similar to the distance between the atomic or molecular structures of interest. Diffraction effects are observed when electromagnetic radiation impinges on periodic structures with geometrical variations on the length scale of the wavelength of the radiation. The inter atomic distances in crystals and molecules amount to 0.15– 0.4 nm which correspond in the electromagnetic spectrum with the wave- length of x-rays having photon energies between 3 and 8 keV. Accordingly, phenomena like constructive and destructive interference should become observable when crystalline and molecular structures are exposed to x-rays.

In order to identify the phase constituents of the weld metal, X-ray diffraction test is performed on the specimen, cut from the weld metal. In Fig.4.36 the diffractive peaks of 1, 2, 3 phase could be observed. It was observed that peaks 1, 2 and 3 formed at 43.6460, 50.758^0 and 74.769^0 respectively.
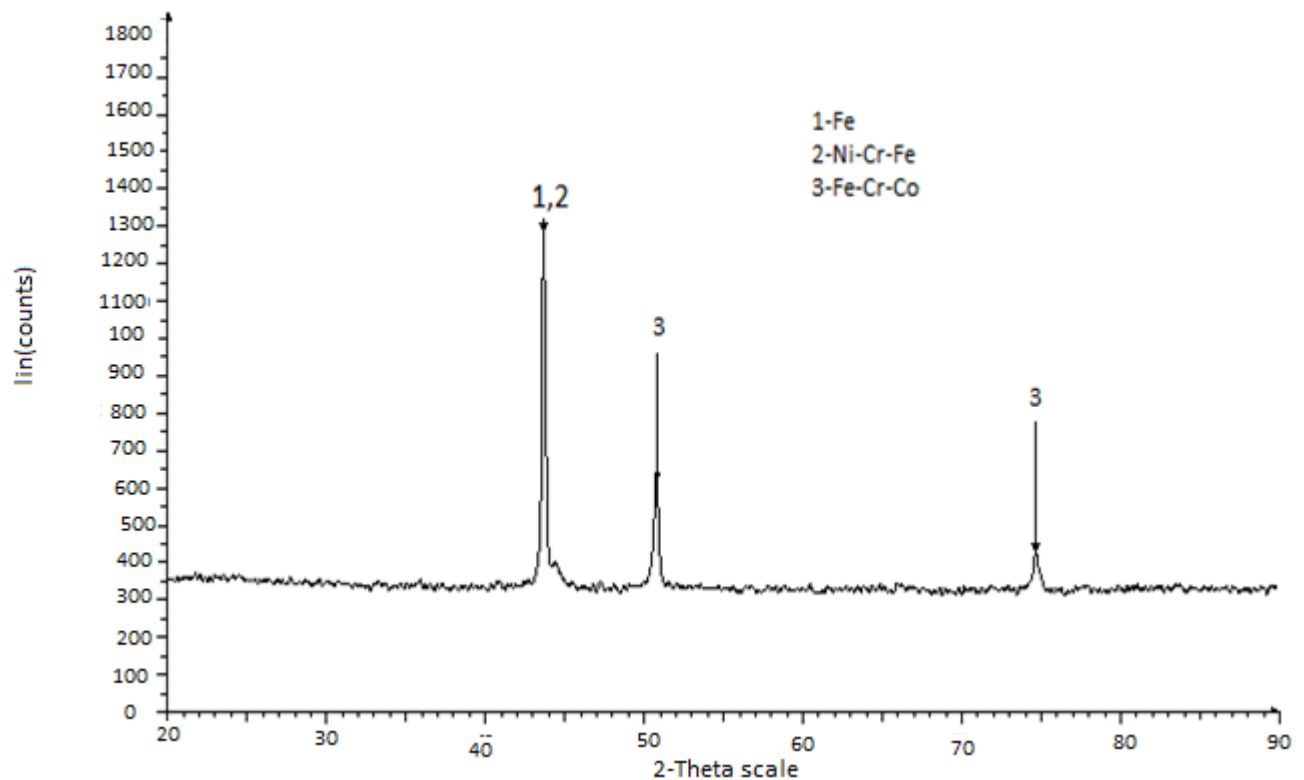
Figure: 4.36 XRD Analysis of welded specimen sample 2

In the XRD analysis, like Fe, Ni-Cr-Fe, and Fe-Cr-Co-Ni phases were determined as shown in above Figure 4.36.

In Fig.4.37 the diffractive peaks of 1, 2, 3 phase could be observed. It was observed that peaks 1, 2 and 3 formed at 43.688^0, 50.719^0 and 74.699^0 respectively
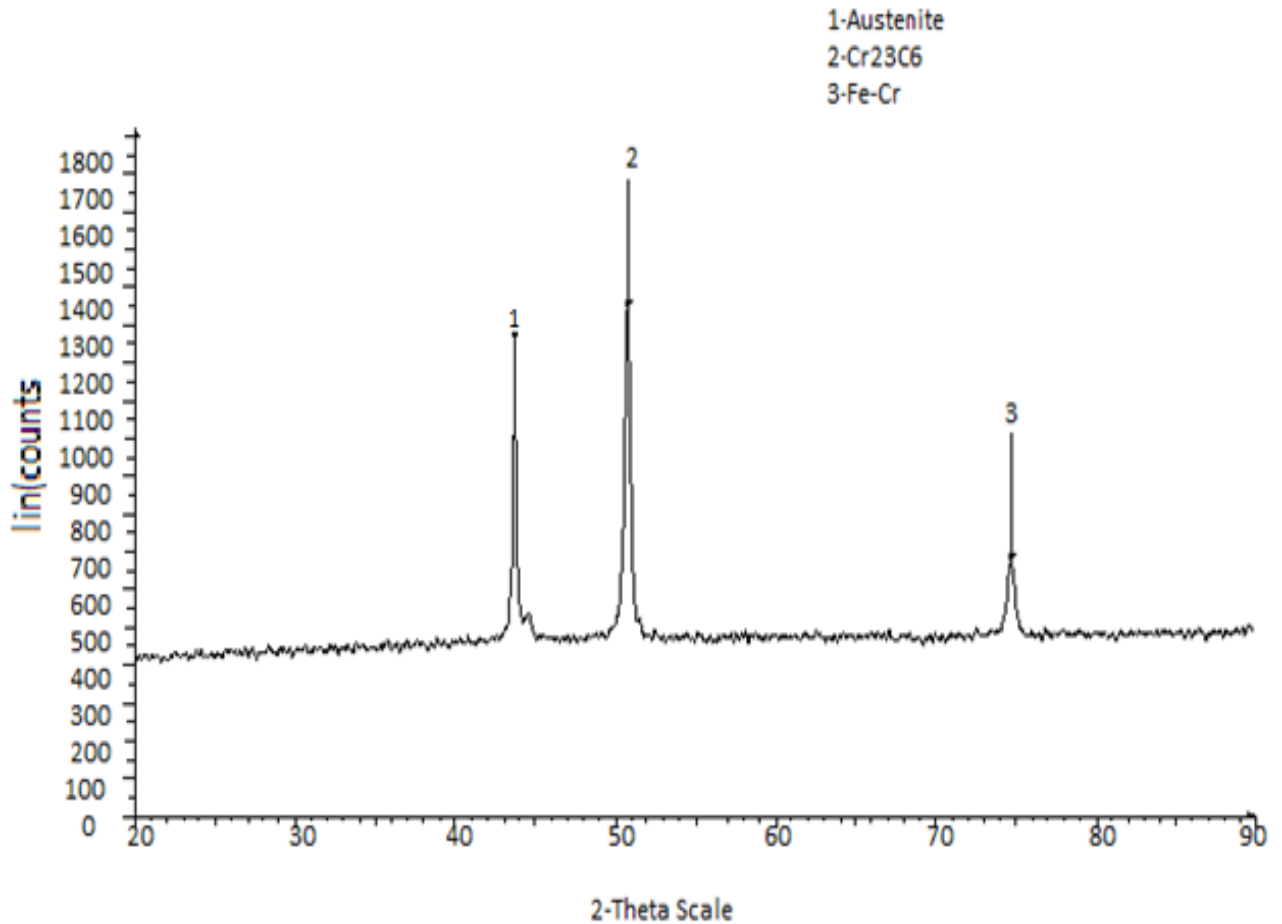

Figure: 4.37 XRD Analysis of the welded specimen sample 4

CHAPTER 5

CONCLUSIONS AND FUTURE SCOPE

The effect of welding parameters as stated previously that has link with arc voltage and filler wire diameter on AISI 304L stainless steel have been investigated.

1. The tensile test of welded sample has been tested on UTM. It was observed that the percentage elongation of welded specimen is 89.126% where as the base specimen is 76.3%. Therefore, the ductility of welded specimen is higher than the base metal.

2. In tensile testing of weld metal, it was also observed that the yield strength and ultimate tensile strength of the weld metal is less than the base metal.

3. Micro hardness has been tested on micro hardness machine Omnitech MVH Auto Micro Hardness tester. It was observed that the hardness value is maximum for base metal and minimum in the HAZ region it is also observed that the hardness values tested at different points in fusion zone is more than hardness value in HAZ region.

4. The flow rate of shielding gas (argon and CO_2) affects micro hardness values of weld metal. The micro hardness increases in the fusion zone with the Increase of gas flow rate.

5. The microscopic study has been done on Olympus GX 41microscope.It was observed that the spatter has been seen for sample 2 and, pin   hole for sample 3, graphite flake columnar has been seen for sample 4.

6. The Microstructure shows precipitation of carbides along grain boundaries which may lead to hardening effect.

7. X ray diffraction (XRD) study has been done and result shows that phases like Fe, Ni-Cr-Fe, and Fe-Cr-Co-Ni are determined.

6. REFERENCES

1. E. Karadeniz, Ozsarac, U. and Yildiz, C. 2007. "The effect of process parameters on penetration in gas metal arc welding process", Materials and Design. Vol 28Issue 2, pp. 649-656.

2. M. Suban and J. Tusek, 2003. "Methods for the determination of arc stability", Journal of Materials Processing Technology, pp. 430-437

3. Jonsson J, Murphy PG, Zeckely AB. 1995 "Influence of oxygen additions on argonshielded gas metal arc welding processes". Weld J;74(2):48s–58s.

4. Chen. TF, Chen YR, Wu W. Properties of Cu–Si enriched type 304 stainless steel welds. Sci Techno Weld Joining 1998; 3:75–9.

5. Yan Jun, Gao Ming, Zeng xiaoyan. Study on microstructure and mechanical properties of 304 stainless steel joints by TIG, laser and laser –TIG hybrid welding. Opt Lasers Eng 2010;48:512-7.

6. Muthupandi V, Srinivasan P Bala, Seshadri SK, Sundaresan S. Effect of weld metal chemistry and heat input on the structure and properties of duplex stainless steel welds. Mater Sci Eng, A 2003;358:9–16.

7. Jana S. Effect of heat input on the HAZ properties of two duplex stainless steels. J Mater Process Technol 1992;33:247–61.

8. Kim I.S., Basu A. and Siores E., 1996 "Mathematical models for control of weld bead penetration in GMAW process". International journal of advanced manufacturing technology, vol 12, pp 393-401

9. D.S. Nagesh, G.L. Datta , Prediction of weld bead geometry and penetration in shielded metal-arc welding using artificial neural networks'' Journal of Materials Processing Technology 123 (2002) 303–312

10. Kim I.S.,Son K.J, Yang Y.S. and Yaragada P.K.D.V.,2003 "sensitivity analysis for process parameters in GMAW process using a factorial design method". International journal of machine tools and manufacture, vol 43,pp736-769

11. Reeta Wattal and S. Pandey Sunil, 2007 "Metal transfer in GMAW of Al alloy

7005." All India Conference on Recent Development in Manufacturing & Quality Management, PEC Chandigarh, 5-6 October, 106-11

12. Zumelzu E, Sepulveda j, Ibarra M Influence of microstructure on the mechanical behavior of welded 316L SS joint. J Mater process Technol 1999:94:36-40.

13. Yan, J. Gao, M. Xeng, X., "Study on microstructure and mechanical properties of 304 stainless steel joints by TIG, laser and laser-TIG hybrid welding, Optics and Lasers in Engineering: 48, 512–517 (2010).

14. El-Batahgy A.M., "Effect of Laser Welding Parameters on Fusion Zone Shape and Solidification Structure of Austenitic Stainless Steels", Materials Letters, 32: 155-163 (1997).

15. Ventrella, V. A., Berretta, J. R., Rossi, W.,"Pulsed Nd: YAG laser seam welding of AISI 316L stainless steel thin foils", Journal of Materials Processing Technology, 210: 1838–1843 (2010).

16. Zambon, A., Ferro, P. and Bonollo, F., "Micro structural, Compositional and Residual Stress Evaluation of CO_2 Laser Welded Super austenitic AISI 904L Stainless Steel", Materials Science and Engineering A, 424: 117- 127 (2006).

17. N. Ames, M. Romberg, M. Johnson, T. Johns, Stainless Steel World©, KCI Publishing BV, 2001.

18. Lee Woei-Shyan, T zeng Fan-T zung, Lin Chi-Feng. "Mechanical properties of 304L stainless steel SMAW joints under dynamic impact loading". J Mater Sci2005; 40: 4839 47.

19. Milad M, Zreiba N, Elhalouani F, Baradai C. The effect of cold work on structure and properties of AISI 304 stainless steel. J Mater Process Technol 2008; 203:80–5.

20. Shyu SW, Huang HY, Tseng KH, Chou CP. Study of the performance of stainless steel A-TIG welds. J Mater Eng Perform 2008; 17:193–201.

21. Ghaini et al., "Weld Metal Micro structural Characteristics in Pulsed Nd: YAG Laser Welding", Scripta Materialia, 56: 955-958 (2007).

22. S.Venugopal, S.L. Mannan, Y.V.R.K. Prasad, Metall. Trans. A23A (1992) 3093.

23. D. Sundararaman, R. Divakar, V.S. Raghunathan, Scr. Metall. Mater. 28 (1993) 1077.

24. S.S. Hecker, M.G. Stout, K.P. Staudhammer, J.L. Smith, Metall. Trans. A 13A (1982) 619.

25. L.E. Murr, K.P. Staudhammer, S.S. Hecker, Metall. Trans. A 13A (1982) 627.

26. Di. Caprio.G, 1997, Gli acciai inossidabili, Ulrico Hoepli Milano, Milano, Italy, pp. 62–89.

27. Eroglu M , Aksoy M , Orhan N,1999, "Effect of coarse initial grain size on microstructure and mechanical properties of weld metal and HAZ of a low carbon steel" Material Science and Engineering; A269: 59-66.

28. P. Ludwik, Phys. Z., Mechanical properties at high strain rates, (1909) 411-417.

29. S.Ganesh Sundara Raman, K.A. Padmanabhan, J. Mater. Sci. Lett. 13 (1994) 389.

30. Mukhopadhyay S, Pal TK. Effect of shielding gas mixture on gas metal arc welding of HSLA steel using solid and flux-cored wires. Int J Adv Manuf Technol 2006;29:262–8.

31. McGrath, J.T., et al., 1988. "Microstructural mechanical property relationships in thick section narrow groove welds". Welding Journal. ;67**:** 196-s–201-s.

32. T. KURSUN, Effect of the gmaw and the gmaw-p welding processes on microstructure, hardness, tensile and impact strength of aisi 1030 steel joints fabricated by asp316l austenitic stainless steel filler metal, 2011, Volume 56,issue.4.

33. Uğur ÇALIGÜLÜ, Microstructural Characteristic of Dissimilar Welded Components (AISI 430 Ferritic-AISI 304 Austenitic Stainless Steels) by CO_2 Laser Beam Welding (LBW), Gazi University Journal of Science*, 25(1):35-51 (2012)*